

Efficiency of weak lensing surveys to probe cosmological models

L. van Waerbeke^{1,2,3}, F. Bernardeau⁴, Y. Mellier^{5,6}

¹ CITA, 60 St Georges Str., Toronto, M5S 3H8 Ontario, Canada.

² MPA, Karl-Schwarzschild-Str. 1, Postfach 1523, D-85740 Garching, Germany.

³ OMP, 14 av. Edouard Belin, 31400, Toulouse, France.

⁴ Service de Physique Théorique. C.E. de Saclay. 91191 Gif-sur-Yvette Cedex, France.

⁵ Institut d'Astrophysique de Paris. 98 bis, boulevard Arago. 75014 Paris, France.

⁶ Observatoire de Paris. DEMIRM. 61, avenue de l'Observatoire. 75014 Paris, France.

December 2, 2024

Abstract. We apply a mass reconstruction technique to simulated large-scale structure gravitational distortion maps, from 2.5 arcmin to 10 degree scales, for different cosmological scenarii. The projected mass is reconstructed using a non-parametric least square method after noise due to the galaxy intrinsic ellipticities has been added on. The shearing of the galaxies is performed using the full lensing equations, without any hypothesis like the weak lensing approximation, or other linearization.

It is shown that, in the reconstructed maps the noise acts as a perfect uncorrelated Poisson noise, with no propagation at large scales. The measured power spectrum and first four moments of the convergence can be corrected accurately for this source of noise. The cosmic variance of these quantities is then analyzed with respect to the density of background galaxies using 60 realizations of each model.

We show that a moderately deep weak lensing survey (5×5 degrees with a typical sheared background population of 30 gal/arcmin² at a redshift $z_s \simeq 1$) is able to probe the amplitude of the power spectrum with a few percents accuracy for models with $\sigma_8 \Omega^{0.8} = 0.6$. Moreover, such a survey would lead to a 6σ separation between open ($\Omega = 0.3$) and flat ($\Omega = 1$) models from the third moment only. This separation is shown to be robust against different hypothesis for the normalization or the shape of the power spectrum, and does not required very deep surveys. The observational strategy for an optimal measurement of the power spectrum and the moments of the convergence is discussed.

Key words: Cosmology: theory, dark matter, gravitational lenses, large-scale structure of Universe

1. Introduction

Mass reconstruction from gravitational distortion inversion is a promising technique to probe the mass distribution and the clustering on very large scales, regardless the nature and the dynamical state of the dark and luminous matter. Pioneered theoretical work done by Gunn (1967), Jaroszyński et al. (1990), Blandford et al. (1991), Miralda-Escudé (1991) and Kaiser (1992) show that the expected distortion amplitude of weak lensing effects produced by large scale mass fluctuations (≥ 1 Mpc) is roughly at the percent level. This low level of distortion is within the possibility of observations due to the large number density of galaxies observed in deep surveys (Kaiser 1992). Needless is to say that the observation of such distortion field provides a unique way to build a picture of the large scale mass distribution, independent on any biasing prescription.

The scientific impact on the determination of cosmological parameters from weak lensing surveys has been underlined by recent theoretical works. Most of the papers previously quoted showed that the distortion two-point correlation function can be used to constrain the mass power spectrum. Villumsen (1996) remarked that the amplitude of the local distortion is proportional to the amplitude of the 3D density fluctuations *and* roughly to the density parameter Ω_0 . Bernardeau et al. (1997, hereafter BvWM) extended these calculations in the $\Omega_0 - \Lambda$ plane and show that the amplitude was also slightly dependent on the cosmological parameter Λ . In the same paper the authors also show that the shape of the convergence probability distribution function can be used to disentangle the Ω and σ_8 dependences for model of large-scale structure formation with Gaussian initial conditions. In particular

they demonstrated that the skewness¹, third moment expressed in terms of the square of the second, is roughly inversely proportional to the total mass density of the Universe Ω_0 , but independent on the amplitude of the fluctuations, as well as the shape of the power spectrum. This result, obtained by means of perturbation theory, is expected to be exact at large enough scale (see Gaztañaga & Bernardeau, 1998), although the skewness is expected to be enhanced in the nonlinear regime at small scales (Gaztañaga & Bernardeau 1998, see also Colombi et al. 1997, and Jain et al. 1998). This effect is actually going to amplify the differences between open and flat cosmologies. So, even if definitive quantitative predictions for such a quantity cannot be given from our present knowledge, it is clear that the skewness can accurately discriminate between different cosmological models.

These theoretical investigations have definitely established the fact that weak lensing survey can be used to determine the power spectrum shape and amplitude, and the density parameter Ω_0 , provided that reliable convergence maps at the percent level can be obtained from the observations.

Since few years many theoretical and observational aspects have been investigated in detail in order to converge toward an unbiased measurement of such small distortions (Bonnet & Mellier 1995, Kaiser et al. 1995, and Van Waerbeke et al. 1997). The technical limitations that have been recognized so far come from systematics caused mainly by the correction of spurious distortions like the optic defects, fuzzy-shaped PSF, and pixel convolution (sampling). Available image analysis techniques and image quality ensure that such systematics can now be reduced to the percent level (it is more than enough for cluster lensing for instance), which is already a great progress compare to what was done four years ago. The ultimate limitation for the use of weak lensing survey as a cosmological probe is therefore dependent on the accuracy with which the correction of the spurious distortions can be corrected. On the other hand, if the systematics can be reduced to the sub-percent level, the limitation of weak lensing analysis is given by the intrinsic ellipticities of the galaxies which acts as a shot noise for the gravitational distortion effect.

In this paper we investigate the effects of this shot noise on the determination of the quantities of interest (cosmological parameters, power spectrum), as well as the effect of having a finite survey (cosmic variance). Two goals are thus looked for,

- what precision on the determination of some cosmological parameters can be expected from such maps;
- what maximum level of observational systematics is acceptable in order to achieve these theoretical precisions.

This study is made in particular in the perspective of ongoing and future wide field deep imaging surveys devoted to weak lensing analysis (for instance the MEGACAM project, Boulade et al. 1998) at CFHT² or the SDSS project, Stebbins 1996). In such a perspective, there are still open questions on the definition of the optimal observation strategy, depending on the scientific goals. Some of the issues are the following:

- In terms of density of lensed galaxies, it is not clear whether deep observations on a small area is really better than a shallow large survey.
- The determination of the optimal shape and size of the survey depends on the noise properties, and on the correlation properties of the signal. The investigations that have been done so far (Kaiser 1992, 1998 and Seljak 1997) assume that the projected mass follows a Gaussian statistics. If such an assumption had to be raised it may significantly change the conclusion that have been reached.

In addition, since the reconstruction of the projected mass from the shape of the galaxies is neither local nor linear in terms of the distortion field (Kaiser 1995) and of the intrinsic ellipticities of the galaxies, it is essential to understand how the noise propagates in the reconstructed mass maps. In order to investigate how these different effects may couple together, we built series of projected mass maps that contain a realistic amount of non-Gaussianity. Then the associated distortion field is derived on the basis of the full non-linear lensing equations. A noise is applied on the distortion maps, and the convergence is then reconstructed. This paper presents the statistical analysis of those reconstructed maps for different cosmological models and different observational contexts.

The sequences of the mass map generation and reconstruction are presented in detail in Sect. 2. It contains also useful definitions. Sect. 3 presents the power spectrum analysis, the noise properties in the reconstructed mass maps, and the cosmic variance on the estimated power spectrum. Sect. 4 repeats similar analysis on moments in real space, where a comparison between top hat and compensated filter is done. It contains also some highlights about other possible statistical quantities that could be used to measure Ω , and a comparison with results obtained for different power spectra. We finally summarize our results and discuss the best observational strategies.

2. Generation of realistic κ -maps

2.1. Lensing effects, displacement and amplification matrix

The physical mechanisms of the gravitational lenses are well known since the foundation of General Relativity. Any

¹ results are explicitly given at beginning of Sect. 4

² See also the WEB page http://terapix.iap.fr/terapix_megacam.html.

mass concentration deflects the photons that are passing by by an angle proportional to the gradient of the local gravitational potential. This effect induces an apparent displacement of the sources, so that a source that was at the angular position ξ^S will be observed at position ξ^I , with

$$\xi^S = \xi^I - \frac{2}{c^2} \frac{\mathcal{D}_K(\chi_s - \chi)}{\mathcal{D}_K(\chi)\mathcal{D}_K(\chi_s)} \int d\chi \nabla\phi(\chi, \xi^I), \quad (1)$$

where χ is the radial coordinate (χ_s is the one of the source), $\mathcal{D}_K(\chi)$ the co-moving angular diameter distance and $\phi(\chi, \xi)$ the 3D gravitational potential. The differential displacement of the images induces an image distortion, which depends on the second derivatives of the gravitational potential, i.e. on the mass density. This gravitational lensing effect of a thin lens is therefore characterized by an isotropic stretching, described by the convergence κ , and an anisotropic distortion given by the complex shear $\gamma = \gamma_1 + i\gamma_2$. The so-called amplification matrix \mathcal{A} that describes the change of local coordinates between the source and image planes, can be expressed with these quantities

$$\mathcal{A} = \begin{pmatrix} 1 - \kappa - \gamma_1 & -\gamma_2 \\ -\gamma_2 & 1 - \kappa + \gamma_1 \end{pmatrix}. \quad (2)$$

Its elements are related to the first derivative of the displacement field,

$$\kappa = \frac{1}{2} (2 - \nabla \cdot \xi^S) \quad (3)$$

$$\gamma_1 = \frac{1}{2} (\nabla_2 \xi_2^S - \nabla_1 \xi_1^S) \quad (4)$$

$$\gamma_2 = -\nabla_1 \xi_2^S, \quad (5)$$

and are therefore related to the projected gravitational potential of the lens ψ via,

$$\kappa = \Delta\psi/2; \quad \gamma_1 = (\psi_{11} - \psi_{22})/2; \quad \gamma_2 = \psi_{12}. \quad (6)$$

where ψ is given by,

$$\psi(\varphi, \chi_s) = \frac{2}{c^2} \int_0^{\chi_s} d\chi' \frac{\mathcal{D}_K(\chi - \chi')}{\mathcal{D}_K(\chi)\mathcal{D}_K(\chi')} \phi(\mathcal{D}_K(\chi')\varphi, \chi'), \quad (7)$$

where φ is the angle such that $\xi = \mathcal{D}_K(\chi)\varphi$. Here ψ depends on χ_s since the potential is integrated from a given source plane χ_s to the observer. This can be trivially generalized to a source redshift distribution. This equation is valid only if the lens-lens coupling is dropped and the Born approximation is used. This is usually not a problem since they have already been demonstrated to have a small contribution in the gravitational lensing effect (see BvWM and Schneider et al. 1997, hereafter SvWJK).

2.2. The galaxy shape matrices

A source galaxy may be described by a complex ellipticity defined as

$$\epsilon^{(s)} = \frac{1-r}{1+r} e^{2i\vartheta} \quad (8)$$

where ϑ is the galaxy orientation, and r is the square of the ratio of the eigenvalues of the shape matrix $Q_{ij}^{(s)}$ of the (centered) surface brightness profile of the galaxy,

$$Q_{ij}^{(s)} = \int d\theta \theta_i \theta_j S(\theta) / \int d\theta S(\theta). \quad (9)$$

In presence of lensing, the shape matrix of the image of the galaxy is given by $Q = \mathcal{A}^{-1}Q^{(s)}\mathcal{A}^{-1}$, and provided that the amplification matrix does not vary over the galaxy apparent area, the observed ellipticity is still described by Eq. (9), and it writes (Schneider & Seitz 1995),

$$\epsilon = \frac{\epsilon^{(s)} - g}{1 - g^* \epsilon^{(s)}} \quad (10)$$

where $g = \gamma/(1 - \kappa)$ is the complex reduced shear. The observable is the distortion $\delta = 2g/(1 + |g|^2)$, but for sub-critical lenses like those we discuss in this work, g is also directly observable,

$$|g| = 1/|\delta| - \sqrt{1/|\delta| - 1}. \quad (11)$$

If the orientation of the source galaxies is random ($\langle \epsilon^{(s)} \rangle = 0$), the observed mean ellipticity of galaxies is an unbiased estimate of the reduced shear (Schramm & Kayser 1995, Schneider & Seitz 1995),

$$\langle \epsilon \rangle = -g. \quad (12)$$

The weak lensing approximation ($\langle \epsilon \rangle \simeq -\gamma$) is generally used in the case of lensing by large scale structures. However, we will not use it since one of the main goals of this paper is to analyze how the noise propagates during the reconstruction of the mass map when the full non-linear Eq. (10) is used.

2.3. Construction of the synthetic projected mass maps, and their reconstruction

The adopted procedure to build and analyze projected density maps is:

1) Generation of a density map, which directly provides the convergence κ given the source redshifts:

In order to make a precise analysis of the cosmic variance and noise properties in the reconstructed mass maps it is necessary to have a large set of simulations of large scale structure. Usual N -body or more elaborated codes are too expensive in CPU time to allow it. Fortunately, it has been showed that second order Lagrangian dynamics (Moutarde et al. 1992) reproduces accurately the statistical characteristics of LSS (Munshi et al. 1994, Bernardeau et al. 1994, Bouchet et al. 1995), and has the main advantage to be very fast numerically. We take advantage of this property to build realistic level of nonlinearities of the projected mass maps using 2D second order Lagrangian dynamics. The cosmology has been included, in order to

compare the ability of the distribution of κ (in particular the skewness of the convergence) to distinguish between low and high density Universes. To this end, the mass fluctuations is normalized to $\langle \kappa^2 \rangle$ rather than $\langle \delta^2 \rangle$, (where δ would be the 3D density contrast). The appendix A gives details about the generation of these maps and how the amount of generated non-Gaussian features compares with real dynamics expectations.

2) Calculation of the associated reduced shear map g and addition of a given level of noise to the reduced shear map:

From the previous projected mass maps, a gravitational distortion map is computed as described in Appendix B. The noise due to intrinsic ellipticities of the galaxies is added using Eq. (10). We are thus left with a map of *observed* ellipticities ϵ which are unbiased estimates of the reduced shear (Eq. (12)). A "high" and "low" noise levels are simultaneously considered which correspond respectively to a mean number density of galaxies of $\bar{n} = 30 \text{ gal/arcmin}^2$ and $\bar{n} = 50 \text{ gal/arcmin}^2$. For the I-band, these number densities are reachable with respectively 1.5 or 4.5 hours exposure at CFHT which is expected to provide galaxies of redshift of about unity. At this stage we have at our disposal a large number of maps that are supposed to mimic accurately what can be observed with large CCD cameras.

3) Reconstruction of the original κ map from ϵ :

This field has known a wide range of development and ramifications (Seitz et al. 1998, Squires & Kaiser, 1996, and references therein). In this work, we use a non-parametric least square method (see Bartelmann et al. 1996 for details) which has the property to over-match the data if no regularization process is used. The hope by doing so is to preserve all the noise properties intact, so that a detailed noise analysis can be done. The κ -field is then reconstructed by minimizing the function,

$$\chi^2 = \sum_{ij} |g_{\text{guess}} + \langle \epsilon \rangle|^2. \quad (13)$$

where g_{guess} is the reduced shear field associated with the unknown potential field. The appendix B gives more technical details about the reconstruction algorithm.

Most of our generated images have an angular size of 5×5 degrees, 120×120 pixels, each pixel having a $2.5'$ angular side (hereafter, the *superpixel* size)³. These are typical scales that a MEGACAM survey at CFHT could probe. Images of size 10×10 degrees (240×240 pixels) have also been generated, in order to estimate how the cosmic variance depends on the survey size in the non-linear regime, and to compare the merit of deep-small survey area versus shallow-large survey. For each cosmological model and observational context series of 60 compact

³ The reason for that pixelisation is that second order lagrangian dynamics is not able to probe high peaks of the density field.

maps are produced. Table 1 gives a summary of the cases that have been investigated.

Table 1. List of the simulations that have been done. The power spectrum BG correspond to the formula (39). It is the same for $\Omega_0 = 1$ and $\Omega_0 = 0.3$. The CDM model corresponds to a standard CDM with $\Gamma = 0.5$. $\bar{\omega}$ is the ratio between the local convergence and the projected normalized density contrast, $\kappa = \bar{\omega} \delta_{2D}$ (see appendix A).

Spectrum	Ω_0	σ_8	z_{sources}	$\bar{\omega}$	size (deg ²)
BG	1.0	0.6	1.0	0.115	5×5
BG	0.3	1.53	1.0	0.045	5×5
BG	1.0	0.6	1.5	0.195	5×5
BG	0.3	1.40	1.5	0.0837	5×5
BG	1.0	0.6	1.0	0.115	10×10
BG	0.3	1.53	1.0	0.045	10×10
BG	1.0	1.0	1.0	0.115	5×5
sCDM	1.0	0.6	1.0	0.115	5×5

Fig. 1 shows two examples of initial κ maps, and the reconstructed mass of the noisy distortion maps. This panel illustrates what MEGACAM should be able to get during only 5 nights (!): 25 exposures in the I band, 1.5 hour each. A single MEGACAM field corresponds to a size of 24×24 pixels on Fig. 1, which is clearly the required minimum area to detect large scale structure features like super clusters, filamentary structures or voids.

3. Power spectrum analysis of the reconstructed maps

3.1. Noise statistical properties of the reconstructed maps

It is clear that the mass reconstruction process does not produce any boundary effects (which is settled by definition). The only boundary effect, slightly detectable on the figure, is a larger level of noise at the border line, due to the change in the finite difference scheme at that position (see Appendix B). The noise due to the intrinsic ellipticities of the galaxies is clearly visible at small scales.

Since the least χ^2 method used to reconstruct the convergence is a local process, it is unlikely that noise propagates on scales larger than the pixel size⁴.

Fig. 3 shows the power spectrum analysis of 60 reconstructed mass maps in the case of two different cosmological models $\Omega = 1$ (cases (a) and (b)) and $\Omega = 0.3$ (cases (c) and (d)). Fig. 3 (a) and (c) show the noise free power spectrum (solid lines) the power spectrum measured on the reconstructed maps with $\bar{n} = 30 \text{ gal/arcmin}^2$ (dotted lines) and for $\bar{n} = 50 \text{ gal/arcmin}^2$ (dashed lines). The plateau for the latter two cases is the consequence

⁴ This is less evident in the case of non-local mass reconstruction.

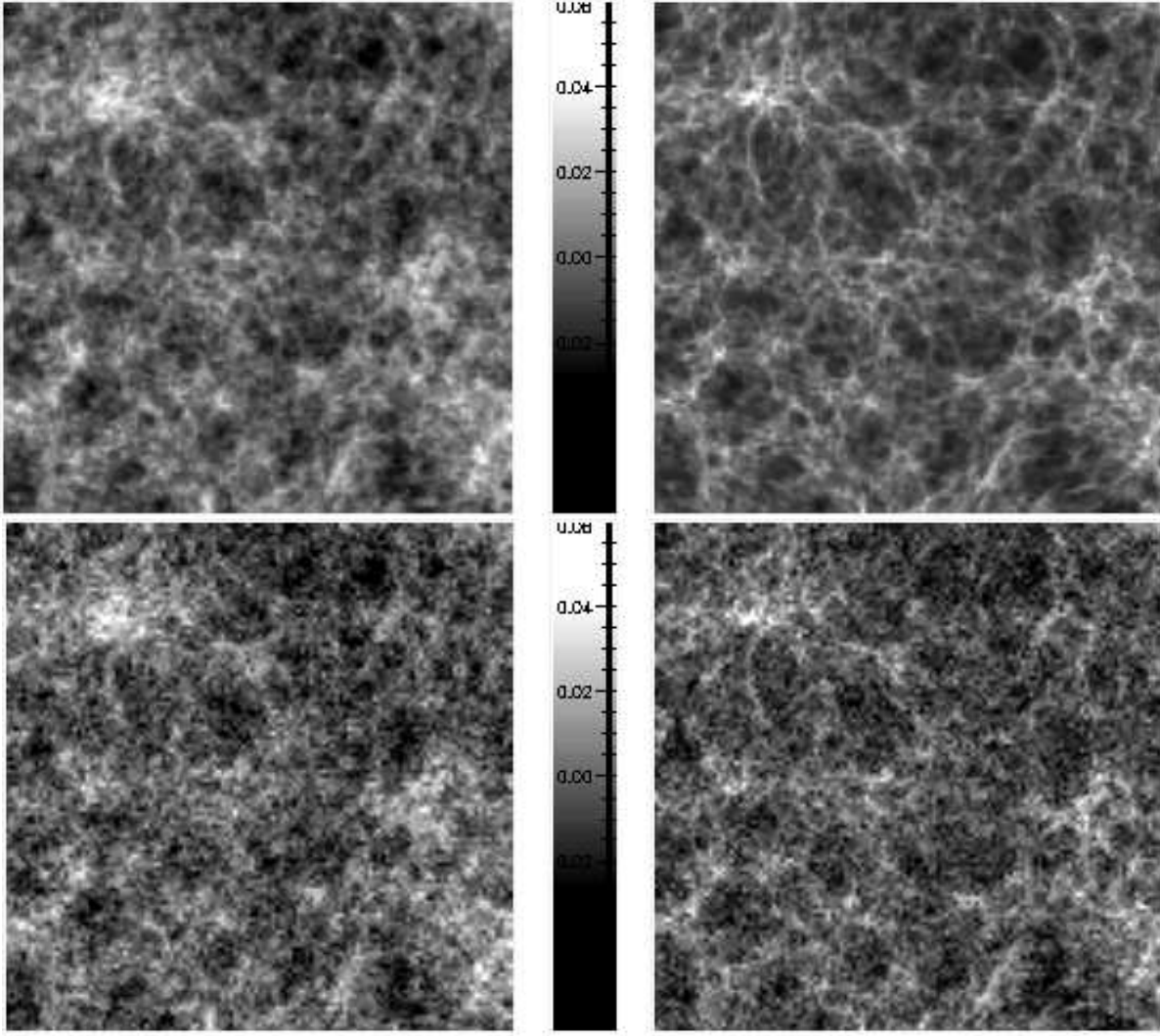


Fig. 1. Example of reconstructions of projected mass maps. The top panels show the initial noise-free κ map for either $\Omega = 1$ (left panel) or $\Omega = 0.3$ (right panel) with the same underlying linear random field (see Appendix A) and the same rms distortion. The bottom panels show the reconstructed κ maps with noise included in the shear maps. The maps cover a total area of 25 degrees². Each pixel has an angular size of 2.5 arcmin² and averages the shear signal expected from deep CCD exposures (about 30 galaxy/arcmin²). The sources are assumed to be all at redshift unity and to have an intrinsic ellipticity distribution given by Eq. (45). Such a survey is easily accessible to MEGACAM at CFHT. The precision with which the images can be reconstructed and the striking differences between the two cosmological models demonstrate the great interest such a survey would have.

of the intrinsic ellipticities of the galaxies: at small scales, the power is dominated by the ellipticity of the galaxies, thus $P(k)$ tends to be constant, generally much more higher than the signal. Figs. (b) and (d) show the difference of the power spectrum measurements on the reconstructed maps with the noise-free power spectrum; thin dotted line is for $\bar{n} = 50$ gal/arcmin² and thin dashed line for $\bar{n} = 30$ gal/arcmin². For visibility, error bars for scales larger than 20 arcmin have been dropped.

In 3D space, these angular scales correspond approximately to scales from 1 to 30 h^{-1} Mpc. We leave for later studies the problem of inverting the measured projected

$P(k)$ to the 3D one. This aspect has already been explored at large angular scale by Seljak (1997).

What are then the statistical properties of the noise? It is, as far as visible on Fig. 3, a pure white noise, superimposed to the initial map. Fig. (2) illustrates the fact that the noise is independent on the underlying κ field and follows a Gaussian distribution. For a more complete understanding of this noise, we compare it to the noise model introduced by Kaiser (1998) based on the weak lensing approximation. When this approximation is applied to Eq. (10) it gives a local shear estimate $\hat{\gamma} = \gamma + \bar{\epsilon}^{(s)}$, where γ is the true shear and $\bar{\epsilon}^{(s)} = 1/N_p \sum \epsilon^{(s)}$, the mean intrinsic ellipticities of N_p galaxies in the superpixel p . Since

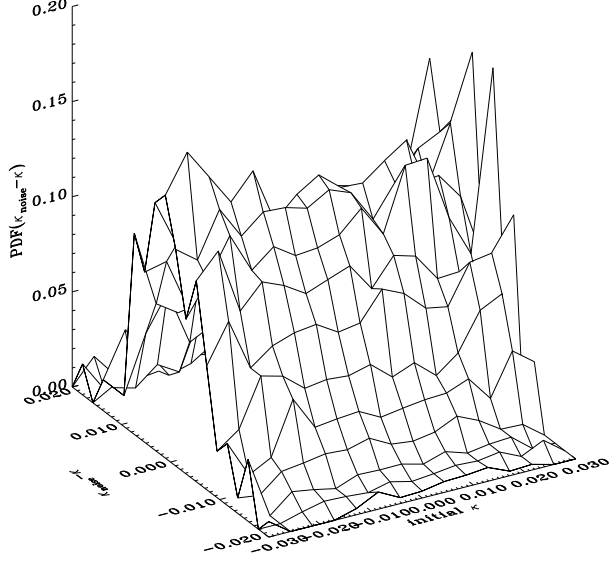


Fig. 2. Histograms of the difference between the noisy mass map and the initial mass map. The values of κ have been selected in bins. The histograms that are found to be all compatible with a Gaussian distribution with a fixed mean and width.

the noise components are assumed to be spatially uncorrelated, the statistical properties of the noise are,

$$\langle \bar{\epsilon}_\alpha^{(s)}(\theta_i) \bar{\epsilon}_\beta^{(s)}(\theta_j) \rangle = \sigma_\epsilon^2 \delta_{\alpha\beta}^K \delta_{ij}^K, \quad (14)$$

where $\alpha, \beta = (1, 2)$, and δ^K is the Kronecker symbol and σ_ϵ is the variance of one component of the intrinsic ellipticities in one superpixel. The shear and the intrinsic ellipticities of the galaxies being uncorrelated in the weak lensing approximation, the measured power (on the noisy mass maps) can be expressed in terms of the true power $P_\kappa(k)$ (the one we want to estimate) and the power spectrum of the noise (Eq.(14)),

$$\langle \tilde{\kappa}^2(k) \rangle \simeq \bar{n} P_\kappa(k) + \bar{\sigma}_\epsilon^2. \quad (15)$$

This equation is only valid for a compact survey, where \bar{n} is the mean number density of the galaxies per superpixel, and $\bar{\sigma}_\epsilon$ is the mean value of σ_ϵ over the survey. For a sparse survey, the first term in Eq. (15) is changed into a convolution term, but the noise contribution to the observed power spectrum remains independent on that power spectrum. A convenient way to estimate $\bar{\sigma}_\epsilon^2$ is to take

$$\bar{\sigma}_\epsilon^2 \simeq \frac{1}{n_{\text{pix}}} \sum_p \left(\frac{1}{N_p} \sum_{\text{gal}} [\epsilon_1^{(s)}]^2 \right), \quad (16)$$

where n_{pix} is the number of superpixels and N_p the number of galaxies in the superpixel p . This is nothing else but the variance of the observed ellipticities of the selected galaxies⁵.

The thick dashed and dotted straight lines on Fig. 3 correspond to the expected noise power spectra (for $\bar{n} = 30 \text{ gal/arcmin}^2$ and $\bar{n} = 50 \text{ gal/arcmin}^2$) according to the Kaiser's model given by Eq. (15). It perfectly fits the noise part of the reconstructed noisy mass maps, whatever the cosmological model, and whatever the noise level. This is true even for the open cosmological models for which stronger non-linearities could have produced a stronger coupling with the noise. The fact that the noise component is pure white noise with an amplitude in agreement with the theoretical prediction is a remarkable result since the full non-linear equations were used, and it shows that the weak lensing approximation can be safely used to remove the noise component and to get an unbiased estimate of the power spectrum, down to the smallest scales considered here.

The behavior at scales smaller than our pixel size remains partly an open issue for two reasons: first, due to the smaller number of galaxies, the convergence of the reconstruction process as well as the stability of the noise properties has to be checked. Second, at small scales the gravitational distortion is larger than only a few percents, and it can even go up to infinity on the critical lines. Thus in order to estimate the variance of the intrinsic ellipticities of the galaxies one should be very cautious to remove arcs and arclets. Our simulations do not allow to address this issue and it has to be done in high resolution simulations like those performed by Jain et al. (1998).

3.2. Power spectrum cosmic variance

Though the estimate of the power spectrum described above is unbiased, it is not sufficient to choose the observational strategy of a survey, and the cosmic variance has also to be explored.

In estimating the cosmic variance of the power spectrum, Gaussian statistics is usually assumed. In order to test the validity of this hypothesis the cosmic variance assuming a Gaussian convergence field will be compared to the true cosmic variance, measured on the simulated mass maps without the noise due to the intrinsic ellipticities of the galaxies. On the same plots, the cosmic variance measured on reconstructed mass maps (including this noise) will be shown.

In the case of Gaussian statistics high order moments are related to the second order moments via the following relations:

$$\langle \tilde{\kappa}(\mathbf{k}_1) \dots \tilde{\kappa}(\mathbf{k}_{2p+1}) \rangle = 0,$$

⁵ The noise depends only on the variance, not on higher moments of the intrinsic ellipticity distribution

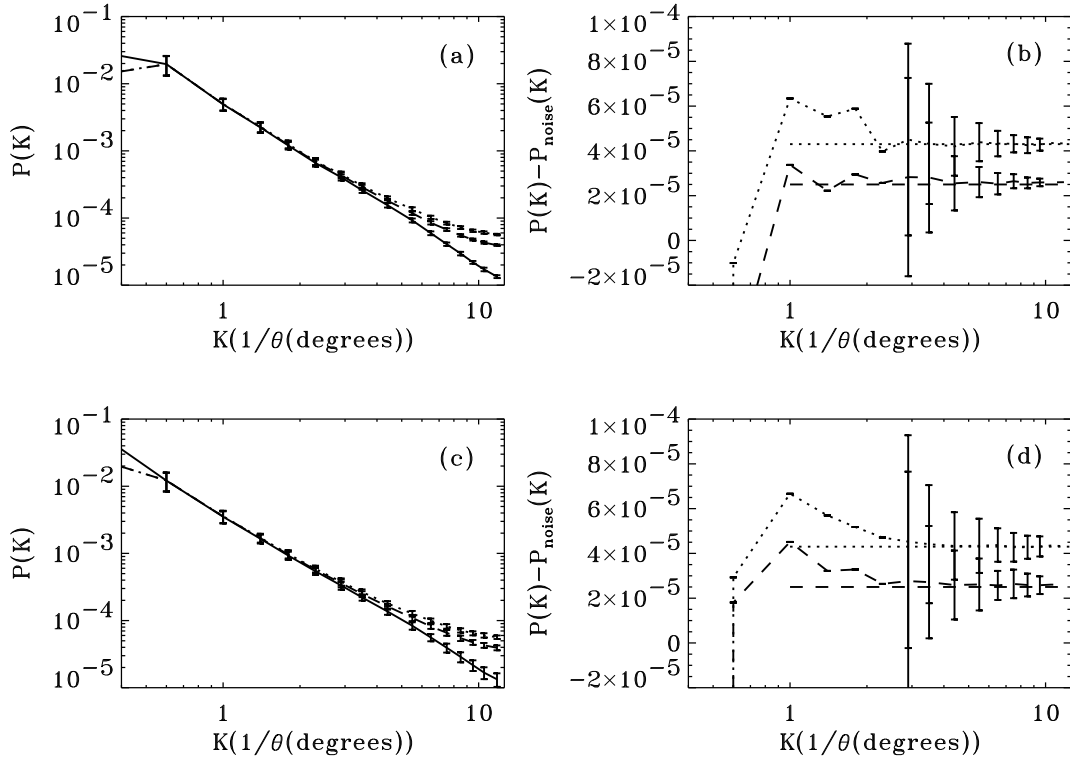


Fig. 3. Power spectrum analysis of the projected density field. The upper series of plots are for $\Omega = 1$ and the lower series for $\Omega = 0.3$. For all the plots, the solid lines show the power spectrum of the noise-free mass maps, before any mass reconstruction. The dotted lines correspond to the power spectrum estimation on the reconstructed noisy maps with a number density of galaxies of $\bar{n} = 30$ gal/arcmin², and the dashed lines for $\bar{n} = 50$ gal/arcmin². The left panels show the power spectrum estimates from the reconstructed noisy maps, compared to the true power spectrum. The right panels show the power contribution due to the noise, it is the difference of power spectra between the reconstructed noisy maps and the true power spectrum. The thick dashed and dotted straight lines show the expected value of the noise contribution in the simple linear noise model described by Eq.(15). It fits remarkably well the true noise level.

$$\langle \tilde{\kappa}(\mathbf{k}_1) \dots \tilde{\kappa}(\mathbf{k}_{2p}) \rangle = \sum_{\text{perm}} \prod_{i=1}^p \langle \tilde{\kappa}(\mathbf{k}_{2i-1}) \tilde{\kappa}(\mathbf{k}_{2i}) \rangle, \quad (17)$$

which means that physically, the frequencies of a Gaussian field are not coupled, and that the $2p$ moment at a given frequency is only determined by the power at that frequency.

We consider a compact survey of size Θ , for which the number of modes available at a frequency is maximum. Thus, following Feldman et al. (1994) and Kaiser (1998), the cosmic variance $\sigma_{P_\kappa}^2(k)$ of $P_\kappa(k)$ is given by the square of the measured signal, $\langle \tilde{\kappa}^2(k) \rangle^2$, divided by the number of independent modes used to determine it, $\Delta N(k)$ in the k -annulus $(k, k + \Delta k)$. Simple modes count gives

$$\Delta N(k) = \pi \frac{k \Delta k}{k_0^2}, \quad (18)$$

where $k_0 = 2\pi/\Theta$ is the fundamental frequency, thus

$$\sigma_{P_\kappa}(k) = \frac{2\sqrt{\pi} \langle \tilde{\kappa}^2(k) \rangle}{\Theta \sqrt{k \Delta k}}. \quad (19)$$

Note that in this hypothesis the cosmic variance is independent on the amplitude of the fluctuations. This is not the case when the non-linear couplings are taken into account as it can be seen in Fig. 4. It shows the cosmic variance for a flat ((a), (c), (d)) and an open (((b), (d), (f))) cosmological model. (a) and (b) corresponds to a 5×5 degrees survey with $z_s = 1$, (c) and (d) with $z_s = 1.5$, and (e) and (f) a 10×10 degrees with $z_s = 1$. On each plot, the thin solid line shows the Gaussian cosmic variance, the thick solid line shows the true cosmic variance without noise, the dotted line the noisy maps with $\bar{n} = 50$ gal/arcmin² and the dashed line with $\bar{n} = 30$ gal/arcmin². The vertical axis gives the error on the power spectrum measured at a given scale.

The departure from Gaussianity appears for scales below $10'$, the effect is however more important in the open case model for which non linearities are stronger. Open models ((a), (c), (e)) give almost the same features as for the flat models (((b), (d), (f))), although the cosmic variance is smaller. This is clearly a consequence of a

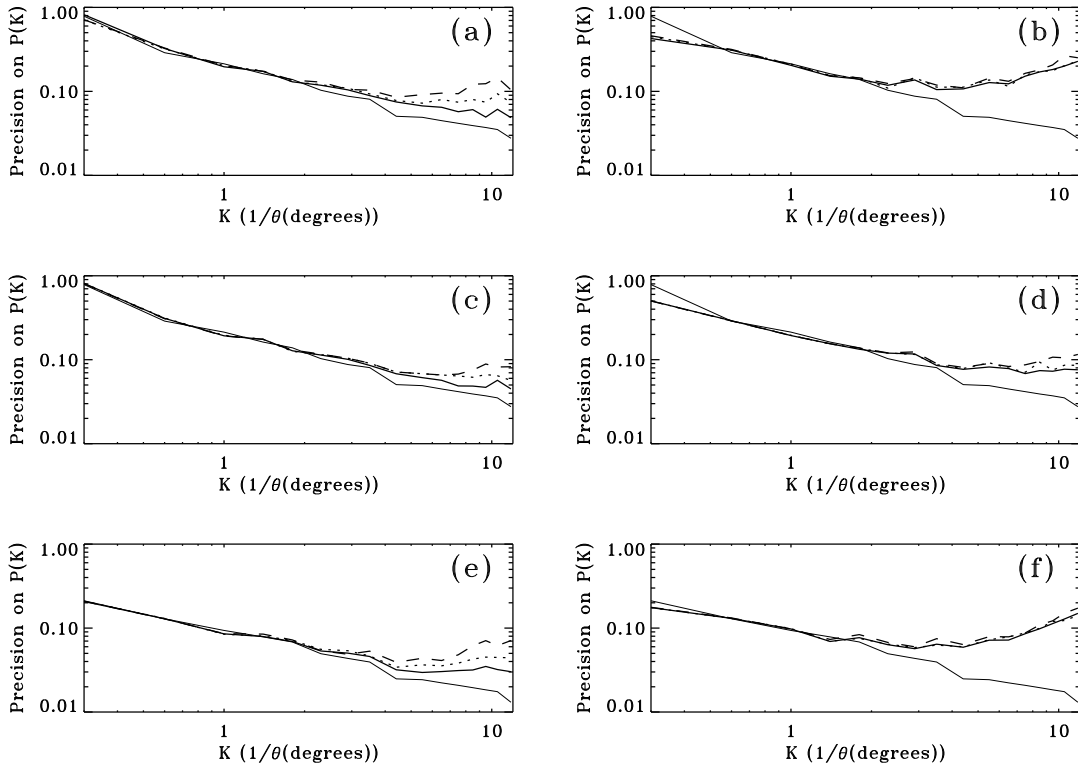


Fig. 4. Cosmic variance for flat (left panels) and open (right panels) models. The thin solid lines are the cosmic variance expected for a Gaussian density field given by Eq. (19). The thick solid lines show the true (measured on the simulations) cosmic variance. The dotted and dashed lines show the cosmic variance on the reconstructed mass maps, respectively with $\bar{n} = 50$ gal/arcmin² and $\bar{n} = 30$ gal/arcmin².

higher power spectrum signal at low scales for these models, which is visible when comparing Fig. 3 (a) (flat) and (c) (open). Thus, as expected, the intrinsic shape of the power spectrum affects the cosmic variance (Kaiser 1998).

Going deep in redshift (by comparing (a) and (c), or (b) and (d) for the open case) clearly improves the cosmic variance at small scale, since the gravitational distortion is stronger. However this stronger distortion does not improve the large scale power estimation because the cosmic variance at these scales only depends on the whole volume survey.

If shorter wave vectors are observed, (for a 10×10 degree survey), which is visualized on (e) and (f), a gain of 2 is reached at all scales, as a direct consequence of global increase of the number of modes in Eq.(18). For small scales, from the point of view of the statistics it is in fact equivalent to observe deep over a small area than to observe shallower over a large area (which reflects the fact that the dashed lines in (e) and (f) ($\bar{n} = 30$ gal/arcmin²) are almost the same as the dotted line in (a) and (b) ($\bar{n} = 50$ gal/arcmin²). But on the other hand, the shallow large survey give a better estimate of the power at large scale than the deep survey. Since these two observational strategies require the same total exposure time

it is clear that wide shallow surveys are better than small deep surveys. Moreover, deep surveys show more and more distant galaxies for which the redshift distribution is more uncertain. As it will be shown in Sect. 4, this remains true for the high order moments in real space.

4. Moments in real space

4.1. Signature of the normalization and non-Gaussian properties

As reminded in the introduction, the scientific interest of weak lensing maps is not limited to the determination of the matter power spectrum. Fig. 1 demonstrates that distortion maps of the same amplitude (and with very similar power spectrum as can be checked in Fig. 2) can display very different features. On these maps the variance of the local convergence is the same, but the amount of non-linearities is very different in the two cases. For low Ω universes, the same amount of distortion can be reached only with a rather large value of σ_8 thus corresponding to a much more evolved dynamics. As a result the difference between the underdense and the overdense regions is more pronounced. The 'voids' tend to occupy a much

larger area, whereas the super clusters tend to be sharper. These features appear because of the non-linear couplings contained in the gravitational dynamics. At large scale the use of Perturbation Theory has proved to be extremely good in predicting the apparition of such properties. All these calculations are based on the hypothesis that the initial conditions were Gaussian. We do adopt the same hypothesis in the following.

It has already been stressed in a previous paper (BvWM) that a way to describe the departure from a Gaussian statistics is to consider the skewness of the probability distribution function (PDF) of the local convergence. In the coming sections we will restrict our analysis on the skewness basically for two reasons: it is beyond the scope of this paper to explore all possible indicators of the non-Gaussian properties, and we know that the approximate dynamics we have adopted reproduces correctly the skewness of the local PDF (see Appendix A). In addition the lens-lens coupling and the Born approximation terms which are known to be small for the third moment are probably more important for higher orders, and this requires a complete dedicated work.

Let us summarize the expected results. For a top-hat window function we expect to have,

$$\sigma_\kappa \approx 0.01 \sigma_8 \Omega_0^{0.8} \left(\frac{\theta_0}{1 \text{deg.}} \right)^{-(n+2)/2} z_s^{0.75}, \quad (20)$$

$$s_3 \equiv \frac{\langle \kappa^3 \rangle}{\langle \kappa^2 \rangle^2} \approx 40 \Omega_0^{-0.8} z_s^{-1.35}, \quad (21)$$

where σ_κ is the rms value of κ at the scale θ_0 , n is the index of the power spectrum, σ_8 is the 3D rms density at $8h^{-1}\text{Mpc}$ scale and z_s is the mean redshift of the sources. The computed skewness s_3 is expected to be independent on the normalization of the power spectrum. It is only weakly dependent on the shape of the power spectrum as well as on the cosmological constant Λ (see discussion). The skewness would then be a very robust way⁶ of determining the density parameter Ω_0 .

Although the moment analysis is generally performed on the basis of a top-hat filter there is a priori no reason to limit our investigations to this filter. In particular SvWJK have proposed the use of an alternative function, the compensated filter that might prove more efficient to constrain Ω , with a lower cosmic variance.

4.2. Top-hat versus compensated filters

Compensated filters were considered by SvWJK as a way to measure the convergence directly from the galaxy

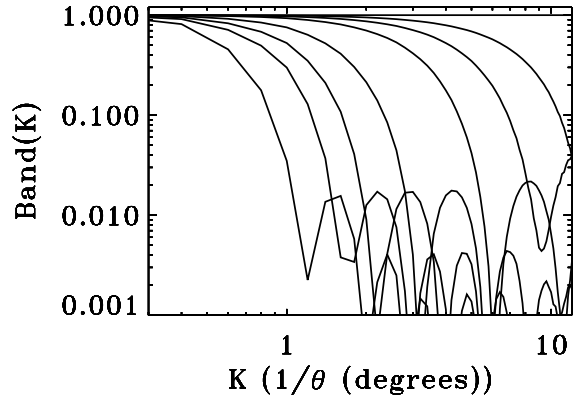


Fig. 5. Spectral response for the family of top-hat filters used in this work.

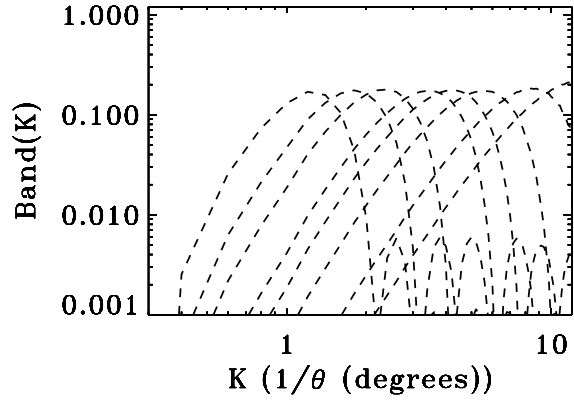


Fig. 6. Spectral response for the family of compensated filters used in this work.

shape. They use the filter $V(\theta)$ of size θ_c that defines the quantity M_{ap} as,

$$M_{\text{ap}}(\theta) = \int_0^{\theta_c} d^2\theta V(\theta) \gamma_t(\theta), \quad (22)$$

where γ_t is the tangential component of the shear field. M_{ap} is nothing else but the convergence field filtered by $U(\theta)$,

$$M_{\text{ap}}(\theta) = \int_0^{\theta_c} d^2\theta U(\theta) \kappa(\theta). \quad (23)$$

where $U(\theta)$ is related to the arbitrary filter V through,

$$V(\theta) = -U(\theta) + \frac{2}{\theta^2} \int_0^\theta d\theta' \theta' U(\theta'). \quad (24)$$

⁶ It is worth reminding that this is only possible if the redshift of the sources are perfectly known (which we assume here).

this latter filter is a compensated filter ⁷ and, for instance, a convenient filter to use is given by,

$$U(\theta) = \frac{3}{\pi\theta_c} \left[1 - \left(\frac{\theta}{\theta_c} \right)^2 \right] \left[\frac{1}{3} - \left(\frac{\theta}{\theta_c} \right)^2 \right]. \quad (25)$$

The spectral responses of the family of filters used in this work, top-hat filter and compensated filter $U(\theta)$, are respectively given by Fig. 5 and by Fig. 6. They are defined as the square values of the Fourier transform of the window functions. Clearly a field smoothed with top-hat filter of size θ_c is sensitive to fluctuations of size larger than θ_c that contribute also to the cosmic variance of the moments. On the other hand, a compensated filter integrates the fluctuation modes only around the target frequency θ_c and any power at lower or larger scales will affect neither the signal nor its cosmic variance. SvWJK showed that the de-correlation properties of compensated filters are by far better than for top-hat filters because any power at small wavelengths between two disconnected field is highly suppressed (see Fig. 8 of their paper). Thus the cosmic variance should be smaller for a compensated filter than for a top-hat filter. However this attractive feature comes with a price: a compensated filter needs to be sampled by a larger number of galaxies. In other words, the shot noise has a larger effect on the aperture mass M_{ap} than on the top-hat filtered mass at the same scale. A compromise has to be found, that depends on the functional shape of the compensated filter and on the shape of the power spectrum.

4.3. Moment estimations and shot noise corrections

Direct estimates of the moments (variance and skewness of M_{ap} and κ in a top-hat) from the reconstructed κ map are biased because of the intrinsic ellipticities of the galaxies (shot noise) and of the cosmic variance (see for instance Szapudi & Colombi 1996, Colombi et al. 1998). However, M_{ap} can be measured using an unbiased estimator based on the measurement of the tangential shear γ_t (see SvWJK), but the measurable quantity is g_t (the tangential reduced shear) rather than γ_t (which has to be corrected for, see SvWJK), and here we will show that the signal to noise of the skewness of M_{ap} is not as good as for a top-hat filter.

It was shown previously that the shot noise leads to a pure white noise in the reconstructed convergence maps. The amplitude of this noise can be obtained by measuring the observed ellipticities of galaxies as described for the power spectrum estimation. Thus estimates of variance and skewness of the convergence in (20) and (21) corrected from the intrinsic ellipticities of the galaxies are obtained

⁷ A compensated filter is a filter with a vanishing mean value. This explains why M_{ap} can be measured only from the distortion field since the mass-sheet degeneracy is removed by the used of this type of filters.

by simply removing the noise term $\langle (\epsilon^{(s)})^2 \rangle$ in the second moment. Note that the skewness correction only requires the correction of the variance since the third moment is not affected by the noise. As the analytical calculation of the noise term for compensated filters can be rather tricky, this is done numerically using Monte-Carlo realizations of noise.

However even after the noise is correctly removed, finite sample effects may also lead to biased estimations of the second moment and of s_3 and to a significant cosmic variance. This effect was partly investigated in BvWM with the use of perturbation theory. It was pointed out that the accessible geometrical averages are expected to be smaller than the true ensemble averages, and that a dispersion is expected in the measurements (cosmic variance):

- the bias that affects the expectation values was found to be proportional to the variance at the sample size divided by the one of at the filtering scale;
- the scatter was found to be proportional to the rms of κ at the sample size.

These estimates were done fully in perturbation theory, with numerous approximations (in particular it was assumed that the sample size was much bigger than the smoothing scale which is probably an erroneous approximation for most of the cases considered here). For accurate investigations of all these effects that take into account both the Poisson noise and the finite volume effects see Szapudi & Colombi (1996).

4.4. Results

We now turn to the measurement of moments in the simulated fields. The same simulations used for the power spectrum analysis are used here. The results are given in Figs. 7 (variance $\langle \kappa^2 \rangle$ in a 5×5 degrees field with $z_s = 1$) and 8 (skewness s_3 in a 5×5 degrees field with $z_s = 1$). For each of these figures the plots are organized in the same way: the first row ((a), (b) and (c) plots) is for the flat model, the second row ((d), (e) and (f) plots) for the open model. It corresponds to the first two rows of Table 1. The first columns (a) and (d) show the estimator measured with a top-hat filter, the second columns (b) and (e) with a compensated filter, and the third columns (c) and (f) show the signal to noise ratio of these estimators. In plots (a), (b), (c) and (d) the solid lines give the estimators measured in the noise-free κ maps, the dotted lines in the noisy reconstructed maps with $\bar{n} = 50$ gal/arcmin² and the dashed lines with $\bar{n} = 30$ gal/arcmin². The dots-dashed lines show the estimators measured on the noisy reconstructed maps with $\bar{n} = 30$ gal/arcmin² corrected from the noise. As the case $\bar{n} = 50$ gal/arcmin² gives the same results it is not plotted. On the signal to noise plots (c) and (f) the thin solid lines show the results for a top-hat filter and the thick solid lines for a compensated filter. The results obtained for the noisy maps with $\bar{n} = 30$ gal/arcmin² or

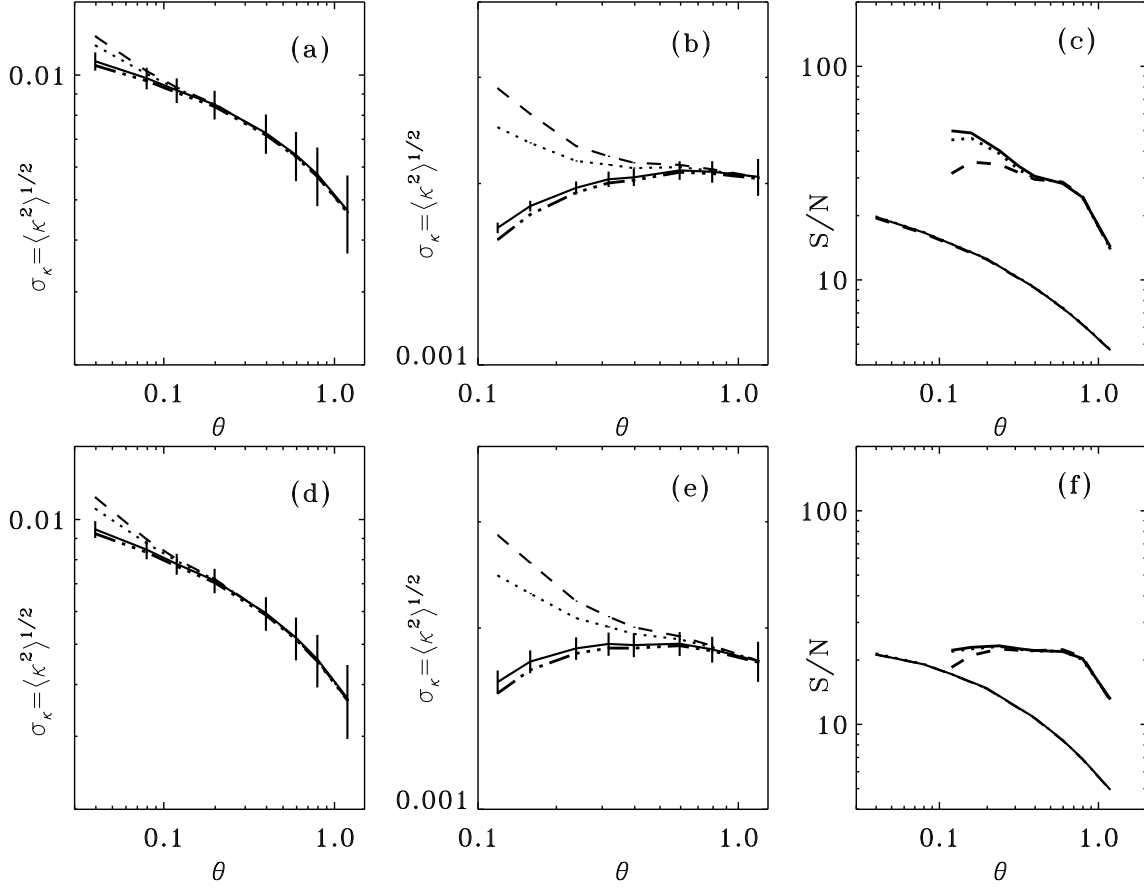


Fig. 7. The measured variance of the convergence, and the corresponding signal to noise ratio. The upper panels show the $\Omega = 1$ case, while the bottom panels correspond to the $\Omega = 0.3$ case. The left and middle panels are respectively the measured variance with a top-hat and a compensated filter. On these plots, the thick solid line is the true variance measured on the noise-free maps, the dashed line and the dotted line for the noisy reconstructed mass maps (with respectively $\bar{n} = 30$ gal/arcmin² and $\bar{n} = 50$ gal/arcmin²). The dots-dashed line is the variance measured from the $n = 30$ gal/arcmin² case and corrected from the noise. The right panels show the signal to noise ratio of the variance detection with the top-hat (thin solid line) and compensated (thick solid line) filters. Dot and dashed lines have the same meaning as for (a), (b), (d) and (e) but here the variance has been corrected from the noise.

$\bar{n} = 50$ gal/arcmin² corrected from the noise are respectively given by the dashed and dotted lines (either thin or thick).

4.4.1. Noise correction

Noise correction as described in Sect 4.3 gives unbiased results, as it is expected for a superimposed white noise. This is true even when the correction is two order of magnitude higher than the signal (see for example Figs. 8 plots (b) and (e)). This confirms the simple properties of the noise in the reconstructed mass maps already found in Sect. 3.1.

4.4.2. The variance

The variance obtained for a top-hat filter is slowly decreasing with, as expected, an increasing scatter. For the compensated filter the curves are almost flat as expected from

the shape of the power spectrum. The noisy maps (dotted and dashed lines in Fig. 7.(a) and (b) display higher values for the variance. Once it is corrected the results are in perfect agreement with the noise-free simulations. The signal to noise ratio is basically not affected by the shot noise for a top-hat filter, it shows that going deep does not improve the measurement precision. The compensated filter reveals much more sensitive to the shot noise as predicted in section 4.2 since we can see on plot Fig. 7. (c) and (f) (thick lines) the bell shape of the signal to noise ratio, with a significant reduction of the measurement precision at the smallest available scales. The open and flat cases show basically no differences. It can be seen however that the signal to noise ratio for a compensated filter is slightly lower for the open case. We interpret this effect as due to the presence of more nonlinear couplings in the maps.

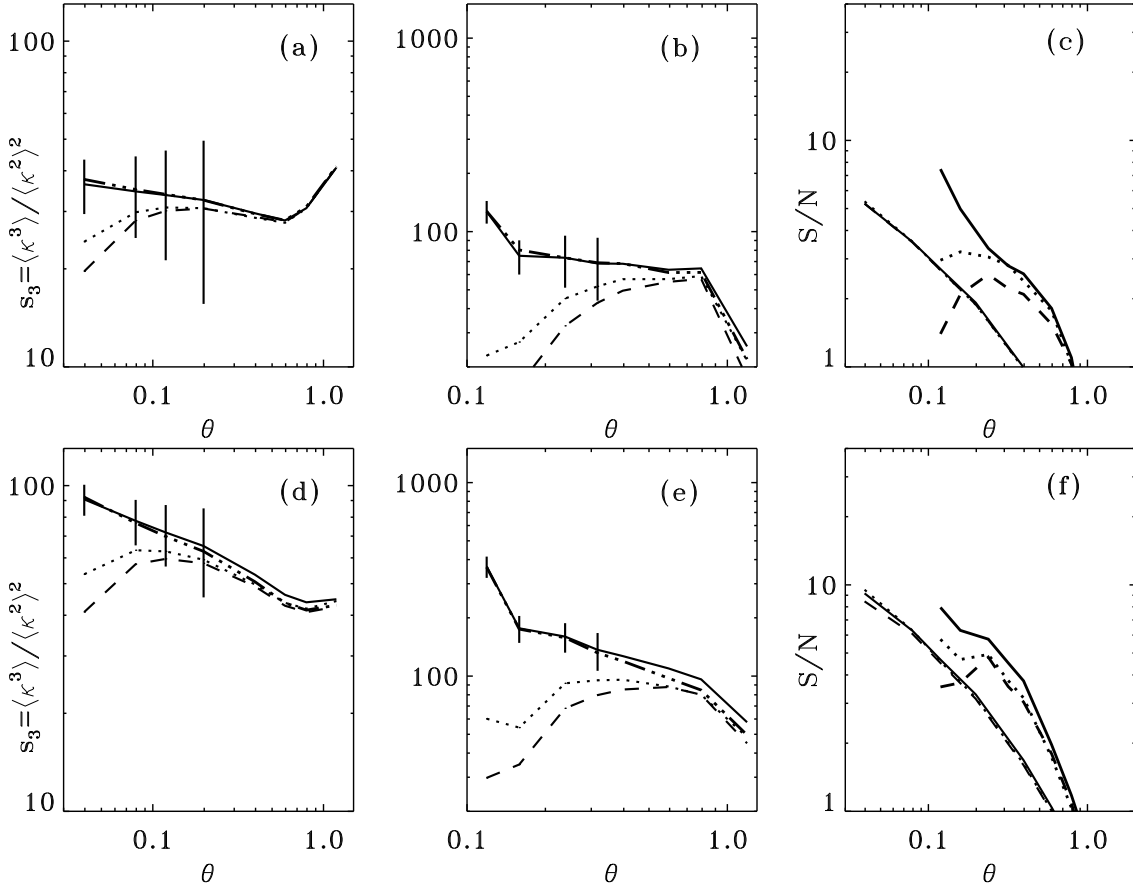


Fig. 8. Same as Fig. 7, but for the skewness of the convergence, s_3 .

Remarkably, the precision with which the variance can be measured in some specific k range reaches 5%.

4.4.3. The skewness

The skewness can be accurately measured at the smallest scales (in Fig. 8 only the error bars for the first four points have been drawn). The skewness is decreasing with scale in the two cases. Once again the noise correction applied to the reconstructed maps allow to recover the skewness with a perfect accuracy. The signal to noise of the skewness is still not affected by the noise for a top-hat filter, while for the compensated filter the situation is worst than for the variance; for instance, at the smallest scale, the signal to noise is almost one order of magnitude smaller on the noisy reconstructed maps than on the noise-free maps for the $\Omega = 1$ case. The two models, open and flat, provide us with very different magnitude for s_3 . They are in ratio about 3 as expected from perturbation theory⁸ results with a significance of the separation at roughly 6σ . This is

⁸ To reduce the cosmic variance, we reject the pixel values that are above 4σ . It slightly reduces the value of s_3 for the open case.

observed in case of the top-hat as well as the compensated filter and this confirms the fact that the skewness of the convergence can strongly separates low and high density universes.

To be more precise we present the actual histograms of the measured skewness in Fig 9 which clearly demonstrate that the two cosmologies are easily separated. One can see that the scatter in s_3 is roughly the same in the two cases and that the difference in the relative precision is due to the differences in the expectation values. This plot also shows that the distribution of the measured s_3 is quite Gaussian.

4.5. Comparisons of different observational scenarios

The results presented previously had been obtained from the full mass reconstruction of 240 maps⁹ as described in Appendix B. But, since it was demonstrated in the preceding section that noise acts as a pure de-correlated white noise in the reconstructed κ maps, we pursue our analysis of large series of simulated fields simply by adding the

⁹ This corresponds to the two noise levels for each cosmological model, with 60 mass maps for each case.

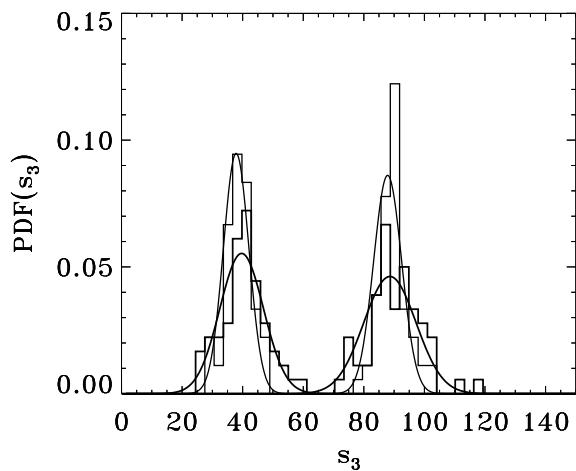


Fig. 9. Histograms of the values of s_3 , top-hat filter, for $\Omega = 1$ and $\Omega = 0.3$ for a 5×5 degree survey (thick lines) and a 10×10 degree survey (thin lines). The angular scale is the pixelsize $2.5'$.

noise on the initial κ maps (especially for 10×10 degrees data sets for which convergence reconstruction would take typically one and half hour on DEC PWS-500 computers). The subsequent analysis are therefore made with this simplified scheme.

To complement the previous cases, we have built and analyzed the cosmic variance on 60 maps for each of the following models: open ($\Omega = 0.3$) and flat ($\Omega = 1$) cosmologies, a survey size of 5×5 degrees for $z_s = 1.5$, a survey size of 10×10 degrees for $z_s = 1$, with the power spectrum of Eq. (39) and a survey size of 5×5 for $z_s = 1$ with a CDM spectrum.

4.5.1. Effect of the survey size

By increasing the total area of a factor 4 we increase the signal to noise on the variance and the skewness with a top-hat filter by almost a factor 1.7. This can be seen on Fig. 9 when comparing the 5×5 degree case with the 10×10 case. With a compensated filter, the signal to noise ratios of the variance and of the skewness are increased by exactly a factor 2, thus improving more rapidly with the sample scale than the top-hat window function. This is expected from the de-correlation properties of those filters. It makes the compensated filter actually more attractive for such a large survey.

4.5.2. Effect of the source redshift

Fig. 10 shows the effect of a change in the mean source redshift. For the galaxies that are further away, the variance of κ is larger since the gravitational distortion is stronger, conversely the skewness is smaller since the accumulated

material along the line of sight creates a field that is more and more Gaussian. The surprising result is that the signal to noise of these quantities does not depends strongly on the redshift of the sources. This means that it will be a waste of time to observe at high redshift, while it will basically not improve the precision of the measurement. Things are slightly improved for the compensated filter, but fundamentally, the results with the top-hat filter show that we do not learn more by going at high redshift. Note that there is no improvement due to the increasing galaxy number density if the survey size is unchanged (see section 4.3). In addition, going at high redshift may creates new problems such as uncertainties due to the Born approximation, the lens-lens coupling or the recently investigated source clustering effect (Bernardeau 1998).

4.6. BG versus CDM power spectrum

In order to test the robustness of the skewness as an estimator of Ω independent on the power spectrum we also ran our simulation machinery for a standard CDM power spectrum. Fig. 11 shows the comparison between the CDM model (dotted line) and BG power spectra, which clearly shows that CDM contains more structures at small scale by looking at the variance plots (a), (b). As predicted in BvWM, the skewness of the convergence is almost unaffected by the change of power spectrum (see Fig. 11 (d), (e)), but a small improvement in the signal to noise for the flat model is visible (because of the larger power at small scale for CDM). On the other hand, the variance is strongly affected by the change, in particular the decrease of power at large scale compare to BG spectrum is clearly visible. Note that the compensated filter, which leads to a more accurate representation of the underlying power spectrum than the top-hat filter (because it is a pass band filter), leaves the angular dependence of the variance unchanged compare to the spectrum Eq.(39) excepts at large scale.

The skewness is thus a robust estimator of Ω fairly insensitive to the power spectrum.

4.7. Effect of the normalization

The skewness s_3 is found to be independent on the normalization, as expected from the Perturbation Theory. The signal to noise ratio however is increased by about 40% in the case of high normalization $\sigma_8 = 1$. These results are summarized in Fig. 12 that shows the histograms in various cosmological cases. It demonstrates that the skewness is clearly independent on the shape and normalization of the power spectrum. However the dependence with the mean redshift of the sources is clearly visible. If the signal to noise ratio for s_3 depends on the cosmology it is independent on the mean source redshift. This again is favoring rather shallow surveys.

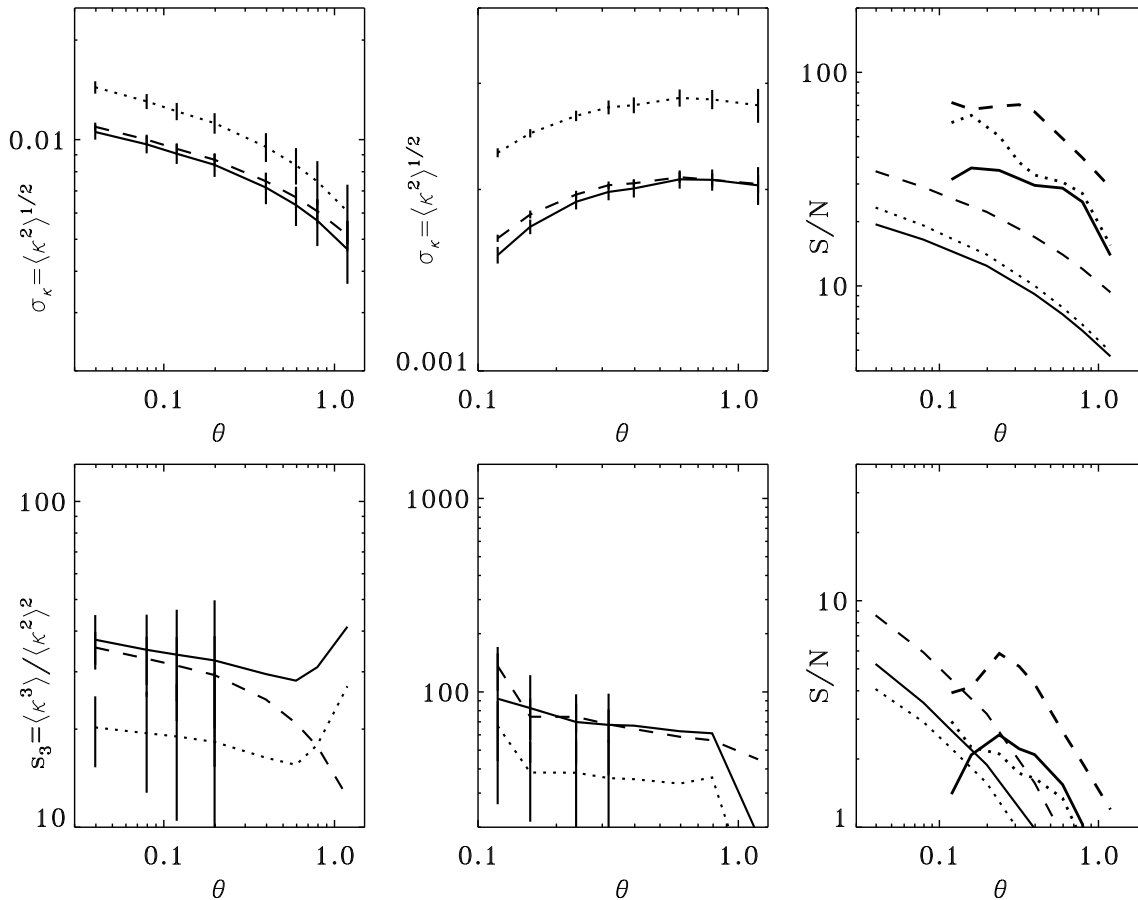


Fig. 10. For a flat cosmological model, comparison of different observational strategies between a survey of size 10×10 degrees (dashed lines) a 5×5 degrees survey for sources at mean redshift 1.5 (dotted lines) and a 5×5 degrees survey for sources at mean redshift 1 (solid lines).

4.8. Beyond the skewness to measure Ω

The way the PDF of the local convergence is skewed does not entirely characterize, by far, this PDF. It would then be natural to try to measure higher order moments of the convergence to probe the cosmology.

Is there any physical reason and interest to search for the kurtosis for example? It is clear that the skewness breaks the degeneracy between the power spectrum and the cosmological parameters, and in addition it is completely insensitive to the normalization. Bernardeau (1995) already noticed that in the case of cosmic density field or cosmic velocity field, the ratio s_4/s_3^2 calculated from the perturbation theory with a top-hat filter is almost a constant, and independent on the underlying cosmological model. This work was recently extended to the lensing case (Bernardeau, 1998) where he found $S_4(\kappa)/S_3(\kappa)^2 \simeq 2$. If all systematics of the gravitational lensing measurement can be controlled, search for such a *magic* number in our Universe would be a strong indication of validity of the paradigm of the gravitational instability scenario started from Gaussian initial conditions.

On the other hand s_4 may be as new way to measure the density parameter (but not totally independent on the skewness). In our maps we found that the noise correction still works for the kurtosis, and that a compensated filter is more efficient than the top-hat filter (at least for noise-free data). In addition the kurtosis appears to be a fairly good discriminant for Ω . Unfortunately the signal to noise ratio remains lower than for the skewness. It means that the kurtosis is certainly more difficult to measure than the skewness. In addition, it is probably more sensitive to the usual lensing approximations (Born approximation and lens-lens coupling terms) as well as source clustering (Bernardeau 1998), which give the preference for the skewness in order to measure Ω . The error bars are so large with a 5×5 degrees size survey that it is impossible to say anything about the kurtosis at scales larger than a few arcmins. It turns out that the ratio $s_4(\kappa)/s_3(\kappa)^2$ is ~ 1.4 for the flat case and ~ 1.8 for the open case for a top-hat filter, while it is ~ 5.6 for the flat case and ~ 3.4 for the open case for a compensated filter. It is not the aim here to go further in the comprehension of these differ-

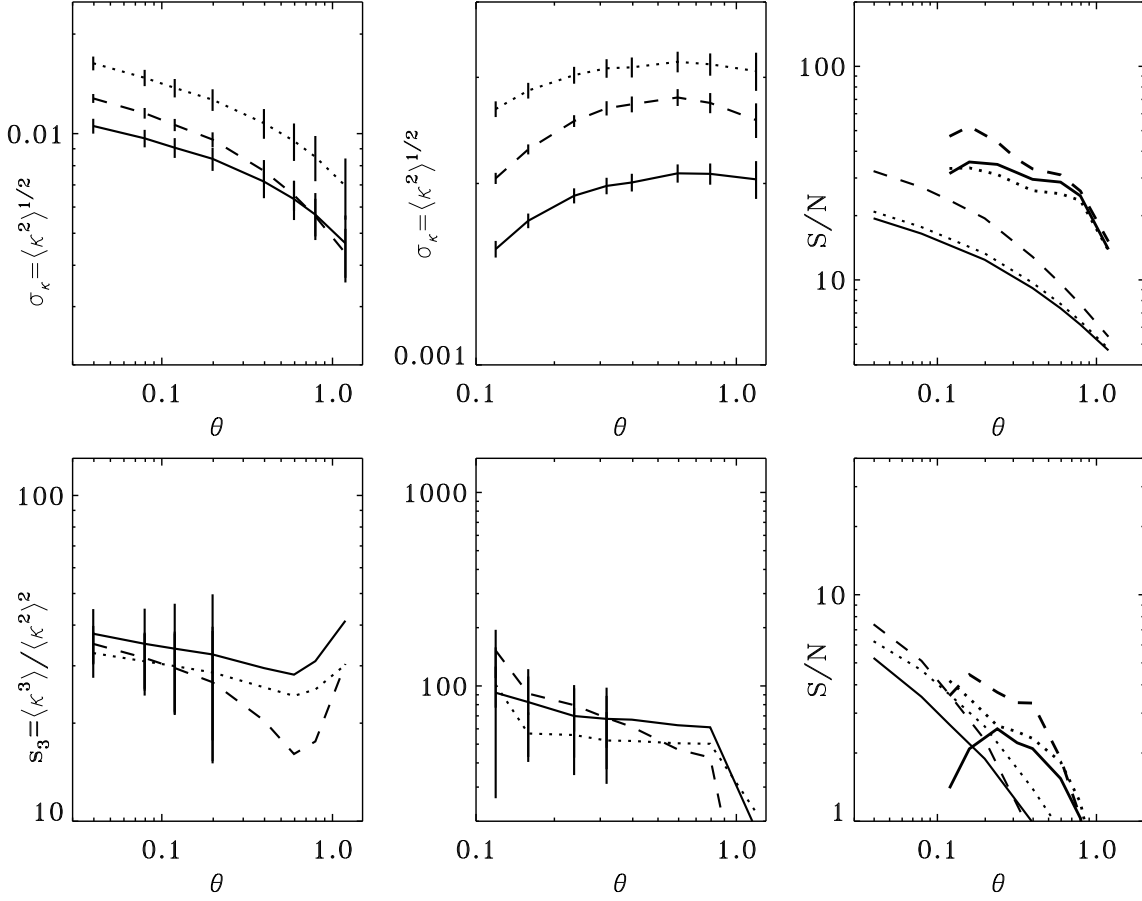


Fig. 11. Direct comparison of different cosmological models for a 5×5 degrees survey and a flat cosmological model. The dashed lines correspond to an $\Omega = 1$ CDM spectrum with $\sigma_8 = 0.6$ and $z_s = 1$, dotted lines to a BG spectrum with $\sigma_8 = 1$ and $z_s = 1$, and the solid lines to a BG spectrum with $\sigma_8 = 0.6$ and $z_s = 1$.

ences between the two filters, but it is worth to note that filtering may be an interesting way to change the dependence of an estimator versus the cosmology, and should be studied in order to search for optimal measures using higher order moments. More generally, the whole shape of the PDF could probably be used with more efficiency than the skewness alone. In a regime of small departure from a Gaussian distribution it can for instance be fruitful to describe the shape of the PDF with an Edgeworth expansion that takes into account the first few moments (Juszkiewicz et al. 1995, Bernardeau & Kofman 1995). For instance, from the edgeworth expansion it is easy to show that the fraction of values of the convergence that is above the average value, $P(\kappa > \langle \kappa \rangle)$, is,

$$P(\kappa > \langle \kappa \rangle) \approx \frac{1}{2} \left(1 - \frac{s_3 \sigma_\kappa}{6\sqrt{2\pi}} \right). \quad (26)$$

The results obtained from this formulae are in good agreement with those obtained from the direct measurement, with however a slightly larger cosmic variance.

And last but not least, beyond the shape of the one-point PDF, the characterization of the non-Gaussian fea-

tures with topological indicators could also be quite fruitful (this is bluming subject in the context of CMB analysis, see for instance Winitzki & Kosowsky 1998, Schmalzing & Gorski 1997). What cosmic variance could be derived from the joint use of topological quantities or/and information on the shape of the PDF is left for further investigations.

5. Discussion

In this paper, we have focussed our investigations on scales larger than $2.5'$ thus allowing ourself the use of a simplified dynamics. This paper appears then to be a complementary approach to the ongoing investigations by Jain et al. (1998) who analyzed the high order moments and the power spectrum of convergence calculated from ray tracing in high resolution simulations. Although they only analyze the statistical properties of the convergence without noise, their approach completes our own towards the smaller angular scales. They have shown in particular that the skewness of the convergence is significantly higher at small scales (0.1 arcmin) than the theoretical expectations

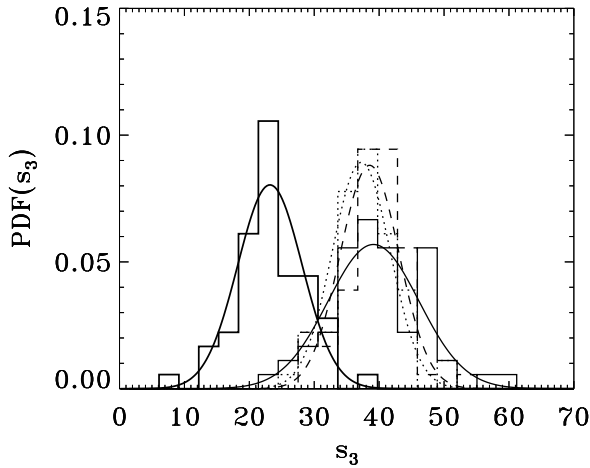


Fig. 12. Histograms of the values of s_3 for 5×5 degree survey, top-hat filter, for $\Omega = 1$ for a BG spectrum with $\sigma_8 = 0.6$ and $z_s = 1$ (thin solid line), $\sigma_8 = 0.6$ and $z_s = 1.5$ (thick solid line), $\sigma_8 = 1.0$ and $z_s = 1$ (dotted line) and a CDM spectrum with $\sigma_8 = 0.6$ and $z_s = 1$ (dashed line). The angular scale is the pixelsize $2.5'$.

of perturbation theory due to highly non-linear structures, (this was already mentioned by Gaztañaga & Bernardeau 1998 and whether this behavior can still be described by means of perturbation theory with the help of loop correction terms is still an open question). Unfortunately, even at these small scales, they are not able to analyze the cosmic variance because of the small number of realizations. The use of high resolution simulations probably prevents a detailed analysis of this quantity.

The preceding sections provide quantitative estimates of the capability of mass reconstruction from weak lensing measurement at large scale to probe the large scale structures, as well as the cosmological parameters. We have shown how the projected mass distribution could be reconstructed accurately from the observed shape of the galaxies. Two complementary analysis have been examined, the power spectrum and the non-Gaussian features through the high order moments.

For the power spectrum estimation, the best sampling strategy (i.e. the question of sparse or compact surveys) is not discussed in this paper (see Kaiser 1998 for a discussion), but our results show that in order to probe the smallest scales of mass fluctuations a deep (but narrow) survey is required that diminishes the cosmic variance caused by the shot noise. Once this is done, the survey can be extended in a more shallower manner to probe the power spectrum at scale where the cosmic variance caused by shot noise becomes unimportant. At this stage, the question of a sparse or compact survey is a matter of choice, depending on scientific interests. However, it is clear that a deep wide survey is a waste of time.

Table 2. Relative error on the measured variance and skewness of the convergence in different observational contexts (in tables $n_1 = 30$ gal/armin² and $n_2 = 50$ gal/armin²) for a top-hat filter. The numbers correspond to the smallest error within the range of scales considered in this work.

Observational constraints		$\Omega = 1$		$\Omega = 0.3$	
		$\delta\sigma_\kappa/\sigma_\kappa$	$\delta S_3/S_3$	$\delta\sigma_\kappa/\sigma_\kappa$	$\delta S_3/S_3$
5×5 deg $z_s = 1$	n_1	0.051	0.190	0.047	0.118
	n_2	0.050	0.186	0.047	0.105
5×5 deg $z_s = 1.5$	n_1	0.043	0.246	0.038	0.127
	n_2	0.043	0.223	0.038	0.123
10×10 deg $z_s = 1$	n_1	0.029	0.116	0.024	0.060
	n_2	0.029	0.110	0.023	0.054

Table 3. Same as Table 2 for a compensated filter

Observational constraints		$\Omega = 1$		$\Omega = 0.3$	
		$\delta\sigma_\kappa/\sigma_\kappa$	$\delta S_3/S_3$	$\delta\sigma_\kappa/\sigma_\kappa$	$\delta S_3/S_3$
5×5 deg $z_s = 1$	n_1	0.028	0.391	0.044	0.209
	n_2	0.021	0.310	0.043	0.174
5×5 deg $z_s = 1.5$	n_1	0.016	0.341	0.030	0.193
	n_2	0.016	0.310	0.029	0.172
10×10 deg $z_s = 1$	n_1	0.014	0.171	0.020	0.110
	n_2	0.014	0.140	0.020	0.074

Concerning the moment measurement, a summary is given in Table 2 (for a top-hat filter) and 3 (for a compensated filter) which shows the smallest accessible error on the measurement of the variance and the skewness of the convergence for different observational contexts. This demonstrates that weak lensing measurements can reach a few percent precision on Ω for a reasonable survey size. It is also important to have in mind that the results are not much deteriorated for a number density of galaxies of 30 gal/armin² compared to 50 gal/armin², whereas the realization of the survey in the latter case requires much more telescope time. It suggests that large shallow surveys would be more adequate since it efficiently reduces the cosmic variance. Such a strategy would be much more comfortable with respect to some systematics like the redshift distribution of the sources (which can be determined easily if the sources are closer), the source clustering effects that are limited if the source distribution is narrow (Bernardeau 1998), and possibly the morphological evolution of distant galaxies, in particular of most distant galaxies are composed of many merging substructures.

Note that there is still room for potential improvement of the signal to noise ratio we are obtaining. Indeed, since we are limited by construction to simulations of scales larger than $2.5'$ we do not know whether the cosmic variance can be reduced by observing the moments at smaller scales, as it is suggested by the results obtained with a

top-hat filter (for which the signal to noise curves never bend down at small scales). The optimal size for the measurement of the variance and the skewness might in fact correspond to the arcmin scale. However, there are several issues that are generally believed to be irrelevant for weak lensing at large scales, but are probably potential difficulties at small scales:

- Our work implicitly assumes a constant power spectrum below the pixel size. A mass reconstruction from real data should include small scale features such as cluster lensing, and the propagation of the noise from this peaks of signal is not known. Moreover that ability of the χ^2 method to match the noise properties correctly at the scales (in order to correct it accurately) should be reinvestigated.
- Born approximation and lens-lens coupling terms are stronger at small scales (see SvWJK). A quantification of this effect on simulations would be necessary to decide at which scale the measurement of moments is optimal.
- Source clustering (investigated at large scales by means of perturbation theory by Bernardeau 1998) could also have a significant impact at small scale.

All these effects should probably be evaluated to be sure that no systematics affect the results at the precision that can be reached with large surveys.

Moreover the moments are not necessary the *best* means to distinguish between different cosmological models (not to mention the fact that the results are anyway filter dependent). For example, it seems that by comparing open and flat Universes on Fig. 1 topological tools should be as well a strong discriminant of cosmological models. The statistical instruments one may consider is however extremely diverse. Among the possible tools the results of multi-scale filtering, as provided by wavelet transforms, is likely to be a good candidate. This is in all cases a difficult problem that is left for further investigations.

6. Conclusion

We have investigated in details how weak lensing observations could be used to measure the projected power spectrum and to discriminate among different cosmological models. In order to analyze the cosmic variance of the results (which requires a large number of realizations), we used a two dimensional, second order Lagrangian dynamics to generate the convergence fields. In each of the observational situation and cosmological model, 60 different maps has been generated. Cosmological models include: flat model ($\Omega = 1$), open model ($\Omega = 0.3$), Baugh & Gaztañaga initial power spectrum, standard CDM spectrum. Observational contexts include: low noise (30 gal/arcmin²) and high noise (50 gal/arcmin²) level, "small" survey size (5×5 degrees) and large survey size (10×10 degrees), two different redshift hypothesis of the

sources ($z_s = 1$ and $z_s = 1.5$), and the use of top-hat and compensated filters. From these convergence maps, a shear map is calculated, on which the noise is introduced according the selected observational context, the mass map is finally reconstructed (using a χ^2 method) and analyzed.

Our findings can be summarized as follow:

- At scales larger than $2.5'$ the χ^2 reconstruction method is a very stable process which does not produce any boundary effects, spurious signal, and which leaves unchanged the noise properties (the noise does not propagates and remains close to the theoretical prediction using the linearized lensing equations). This provides a unique way to work with the convergence (which is the physical field of interest) instead of the shear, with no loss of information.
- The shot noise contribution can be removed simply by measuring the *observed* ellipticities of the galaxies, and this leads to unbiased estimates of the power spectrum and the moments of the convergence (at least up to the kurtosis).
- The precision obtained on the normalization can be as low as 2% with survey of 10×10 , and 5% for Ω (see tables 1 and 2) for the most favorable cases (i.e. low Ω).
- It seems more productive to make a 10×10 shallow survey than a 5×5 deep survey. This has other advantages: the redshift distribution will be better known and galaxies have less clumpiness than at high redshift making it easier to characterize their shapes.
- The compensated filter gives by far smaller cosmic variance than the top-hat filter for the variance of the convergence, while it gives bad results for the skewness. However the cosmic variance decreases more rapidly with an increasing survey size for a compensated filter.

The MEGACAM project offers the possibility to perform these observations. Indeed the large field of the CCD device (1 square degree) and the high image quality at CFHT (extended to the edges of the field with the future field corrector) provides the ideal instrument to fulfill such a scientific program.

In the context of the rapid changes occurring in observational cosmology it is worth stressing that weak lensing surveys offer precious complementary views of our Universe. The perspective of determining the projected power spectrum independently of biases is indeed attractive. Moreover the possibility of determining Ω_0 in a way which is independent on the power spectrum, and independent on all the methods that have been suggested so far, is also extremely precious. We remind that this determination relies only on dynamical effects assuming that the large-scale structures originate from Gaussian initial conditions through gravitational instabilities. In Fig. 13 examples of constraints in the (Ω, Λ) plane with weak lensing

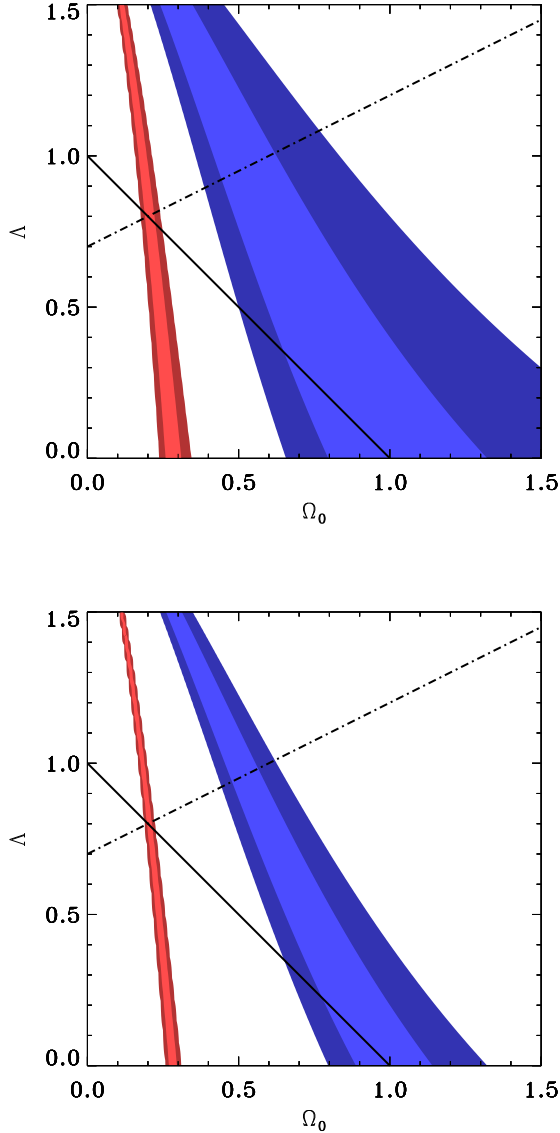


Fig. 13. Constraints that can be brought by weak lensing survey in an $\Omega_0 - \Lambda$ plane. The grey bands are the location of the 1 and 2- σ locations (respectively darker and lighter bands) allowed by a measured skewness that would be obtained with either $\Omega_0 = 0.3$ (left bands) or $\Omega_0 = 1$ (right bands). The solid straight lines corresponds to a zero curvature universe, and the dot-dashed lines to a fixed acceleration parameter, q_0 . The panels correspond to survey of either 5×5 (top) or 10×10 degrees (bottom).

as describes in this work (shaded areas) are presented¹⁰ together with the location of the major constraints that are expected to be brought either with CDM experiments, (constant curvature density, solid lines), or from Supernovae Ia measurements (the other straight lines, describing constant q_0 values).

If it is true that the future CMB experiments can determine the cosmological parameters with a remarkable accuracy, this is possible only when some prior is put on the shape of the initial power spectrum. The curvature will probably be determined with a good accuracy in the near future from the position of the first Doppler peak on the C_l curves. But it appears that it can be very difficult to disentangle Ω_0 from Λ (see for instance Zaldariagga, Spergel & Seljak 1997) from the mere temperature (and polarization) fluctuations. This is only possible from very detailed analysis and the power spectra which require not only a good understanding of the possible systematics that may affect the measurements, but also specific hypothesis on the regularity of the primordial power spectrum. The requirements to measure Ω_0 from weak lensing survey are less strict provided the instrumental systematics can be correctly controlled.

Moreover weak lensing survey should also be able to get significant constraints on Λ if it is possible to select efficiently several populations of sources (see Villumsen 1996, BvWM for clues of such possibilities).

The feasibility of the weak lensing by large scale structure program and the full scientific exploitation of its possibilities is now almost reduced to our capability to control instrumental systematics. As reminded in the introduction, several issues are still crucial in that program. The most dedicated problem comes probably from the need of a PSF correction to avoid artificial large scale coherent alignments of galaxies. A systematic small error in the correction would inevitably produce spurious signals. Related to this problem is the pixelisation effects. Galaxies shapes are indeed determined from a finite number of pixels with the possible introduction of errors and biased estimation on the shapes (that can depend as well on the orientation of the galaxies).

These effects can all be investigated independently. Taking several images of the same portion of the sky with a shifted position for the camera, or with different cameras would definitely test the robustness of the observed distortion maps. Moreover we have at our disposal numerous statistical tests that can be done on the maps: comparison of the 2-point correlation function of the distortion with the one of the shear field or with the one of the κ field, or even by the investigation of quantities that are a priori sensitive to the systematics in a different manner, such as the correlation of the orientations of the distortion field. That all these quantities have related properties is

¹⁰ The Λ dependence is taken from the theoretical results given by BvWM.

somehow due to the fact that in the thin lens approximation the γ field should be irrotational (see for example Luppino & Kaiser 1997 for a used of these tests). This is true only when lens-lens couplings are neglected but it should be possible to investigate those effects in numerical simulations.

Acknowledgements. It is a pleasure to thanks S. Colombi for his useful suggestion to use a second order Lagrangian dynamic, B. Fort, P. Schneider, B. Jain and U. Seljak for fruitful discussions. This work was supported by the Programme National de Cosmologie and the “Sonderforschungsbereich 375-95 für Astro-Teilchenphysik” der Deutschen Forschungsgemeinschaft. L.V.W. and F.B. thank IAP, where a fair fraction of this work has been done, for hospitality.

References

- Bartelmann M., Narayan R., Seitz S., Schneider P. 1996, ApJ 464, 115
- Baugh C. M., Gaztañaga E. 1996, MNRAS 280, L35
- Bernardeau F. 1998, A&A accepted, astro-ph/9712115
- Bernardeau F. 1995, A&A 301, 309
- Bernardeau F., Kofman L. 1995, ApJ 443, 479
- Bernardeau F., Singh T.P., Banerjee B., Chitre S.M. 1994, MNRAS 269, 947
- Bernardeau F., Van Waerbeke L., Mellier Y. 1997, A&A 322, 1
- Blandford R. D., Saust A. B., Brainerd T. G., Villumsen J. V. 1991, MNRAS 251, 600
- Bonnet H., Mellier Y. 1995, A&A 303, 331
- Bouchet F., Colombi S., Hivon E., Juszkiewicz R. 1995, A&A 296, 575
- Bouchet F., Colombi S., Juszkiewicz R., Pellat R. 1992, ApJ 394, L5
- Boulade O., Vigroux L., Charlot X., et al. 1998, “MEGACAM, the next Generation Wide-Field camera for CFHT”. SPIE Vol. 3355, “Astronomical Telescopes and Instrumentation”, Kona Hawaii, March 1998
- Colombi S., Bernardeau F., Bouchet F., Hernquist L. 1997, MNRAS 287, 241
- Colombi S., Szapudi I., Szalay A. 1998, MNRAS 296, 253
- Eke V., Cole S., Frenk C. 1996, MNRAS 282, 263
- Feldman H. A., Kaiser N., Peacock J. A. 1994, ApJ 426, 23
- Gaztañaga E., Bernardeau F. 1998, A&A 290, 566
- Gunn J.E., 1967, ApJ 150, 737
- Jain B., Seljak U., White S.D.M., astro-ph/9804238
- Jaroszyński M., Changbom P., Paczyński B., Gott J.R. 1990, ApJ 365, 22
- Juszkiewicz R., Weinberg D., Amsterdamski P., Chodorowski M., Bouchet F.R., 1995, ApJ 442, 39
- Kaiser N. 1992, ApJ 388, 272
- Kaiser N. 1995, ApJ 439, L1
- Kaiser N., Squires G., Broadhurst T. 1995, ApJ 449, 460
- Kaiser N. 1998, ApJ 498, 26
- Luppino G., Kaiser N. 1997, ApJ 475, 20
- Oukbir J., Blanchard A. 1997, A&A 317, 1
- Moutarde F., Alimi J.M., Bouchet F., Pellat R., Ramani A. 1991, ApJ 382, 377

- Munshi D., Bernardeau F., Mellot A.L., Schaeffer R. 1997, astro-ph/9707009
- Munshi D., Sahni V., Starobinsky A.A. 1994, ApJ 436, 517
- Seljak U. 1997, astro-ph/9711124
- Schmalzing J., Gorski K. M., astro-ph/9710185
- Schneider P., Seitz C. 1995, A&A 294, 411
- Schneider P., Van Waerbeke L., Jain B. Kruse, G. 1997, MNRAS accepted, astro-ph/9708271 (SvWJK)
- Schramm T., Kayser R. 1995, A&A 299, 1
- Seitz S., Schneider P., Bartelmann M. 1998, astro-ph/9803038
- Squires G., Kaiser, N. 1996, ApJ 473, 65
- Stebbins A. 1996, astro-ph/9609132
- Szapudi I., Colombi S. 1996, ApJ, 470, 131
- Van Waerbeke L., Mellier Y., Schneider P., Fort B., Mathez G., A&A 317, 303
- Villumsen, J.V., 1996, MNRAS 281, 369
- Winitzki S., Kosowsky A., astro-ph/9710164
- Zel’dovich Y. B. 1970, A&A 5, 84

Appendix A: Second order Lagrangian dynamics

In order to investigate the statistical properties of the reconstructed mass field that contains a significant amount of non-linearities, a non-linear evolution model of large-scale structures is required. Second order Lagrangian perturbation theory has the advantage to be extremely fast to compute, and rather accurate compare to N-body simulations. It gives correct values for the skewness S_3 and we expect it to correct estimation of the cosmic variance (see Munshi et al. 1994, Bernardeau et al. 1994, Bouchet et al. 1995).

Actually we do not even need to do 3D simulations. At the level of perturbation theory it is equivalent to perform 2D second order Lagrangian evolutions of the structures on an initial linear map of the projected mass fluctuations.

Construction of the initial linear map

The local convergence map is given by,

$$\kappa(\varphi) = -\frac{3}{2} \Omega_0 \int_0^{\chi_H} d\chi_s n(\chi_s) \int_0^{\chi_s} d\chi \frac{\mathcal{D}_K(\chi_s - \chi) \mathcal{D}_K(\chi)}{\mathcal{D}_K(\chi_s)} \frac{\delta(\mathcal{D}_K(\chi)\varphi, \chi)}{a} \quad (27)$$

where χ_H is the horizon distance, Ω_0 the density parameter, a the expansion factor and $n(\chi_s)$ the number density of sources as a function of the distance χ . For clarity we introduce the lens efficiency function,

$$w(\chi) = \frac{3}{2} \Omega_0 \int_\chi^{\chi_H} d\chi_s n(\chi_s) \frac{\mathcal{D}_K(\chi_s - \chi) \mathcal{D}_K(\chi)}{a \mathcal{D}_K(\chi_s)}, \quad (28)$$

so that the local convergence is simply given by the integral over the line of sight of,

$$\kappa(\varphi) = - \int_0^{\chi_H} d\chi w(\chi) \delta(\mathcal{D}_K(\chi)\varphi, \chi). \quad (29)$$

The projected density contrast would then identify with,

$$\delta_{2D} = \frac{\kappa}{\bar{\omega}} \quad \text{with} \quad \bar{\omega} = \int_0^{\chi_H} d\chi w(\chi). \quad (30)$$

It is important to keep in mind that the local convergence is related to the actual density contrast with a constant that depends on the cosmological parameters. In the following we will assume that all sources are at the same redshift (it is not realistic but of no consequences on our results here).

In the linear approximation the κ field is expected to be a 2D Gaussian field, characterized by a power spectrum, P_κ , with (see Kaiser 1992, 1996, and SvWJK)¹¹,

$$P_\kappa(k) = \int_0^{\chi_H} d\chi w(\chi)^2 P_\delta\left(\frac{k}{\mathcal{D}_K(\chi)}, \chi\right), \quad (31)$$

as a result of the relation between κ and the 3D density contrasts. The initial conditions for κ are therefore generated by a 2D Gaussian field in Fourier space where the complex random variables verify

$$\langle \tilde{\kappa}(\mathbf{k}) \tilde{\kappa}^*(\mathbf{k}') \rangle = (2\pi)^2 \delta_D(\mathbf{k} - \mathbf{k}') P_\kappa(k), \quad (32)$$

The 2D second order Lagrangian dynamics

In order to introduce a significant amount of nonlinearities in the maps, we apply the 2D second order Lagrangian dynamics to the projected density, δ_{2D} . Following the notations of Bouchet et al. (1992), transposed in the 2D case, let us write the 2D Eulerian coordinates $\boldsymbol{\theta}(\mathbf{q})$ as a perturbation series over the 2D displacement field \mathbf{D} ,

$$\boldsymbol{\theta}(\mathbf{q}) = \mathbf{q} + \epsilon \mathbf{D}^{(1)}(\mathbf{q}) + \epsilon^2 \mathbf{D}^{(2)}(\mathbf{q}) + o(\epsilon^3), \quad (33)$$

where \mathbf{q} is the angular Lagrangian coordinates and ϵ a small dimension-less parameter. The first order term reduced to the Zel'dovich (Zel'dovich 1970) approximation. The divergence of the second order displacement field can be written in terms of the first order solutions,

$$\mathbf{D}_{i,i}^{(2)}(\mathbf{q}) = \frac{3}{7} \left[\mathbf{D}_{1,1}^{(1)} \mathbf{D}_{2,2}^{(1)} - \left(\mathbf{D}_{1,2}^{(1)} \right)^2 \right]. \quad (34)$$

This result is exact for an Einstein-de Sitter Universe. The values of the coefficient 3/7 is only slightly altered (about 1%) for other cosmological models (Bouchet et al. 1992, Bernardeau 1994) and in the following we did not take into account this dependence. Once the second order displacement field has been computed, the local 2D density contrast can then be written in terms of the Jacobian of the transform between the Lagrangian coordinates and the Eulerian coordinates,

$$\delta_{2D}(\boldsymbol{\theta}(\mathbf{q})) = \frac{1}{J(\mathbf{q})} \quad (35)$$

¹¹ Taking $H_0 = c = 1$.

where $J = |\partial\theta_i/\partial q_j|$. The local convergence is then given by,

$$\kappa(\boldsymbol{\theta}(\mathbf{q})) = \bar{\omega} \delta_{2D}(\boldsymbol{\theta}(\mathbf{q})). \quad (36)$$

The linear density maps are built on a regular grid from random modes following a given power spectrum. The different quantities up to the Jacobian are generated on this same grid by successive Fast Fourier Transforms. There is then a technical difficulty to solve in order to get the resulting values of κ on a regular grid. This is done via a local triangulation and an interpolation of the values (from standard IDL packages). The amplitude of the fluctuations is such that the displacement field does not induce shell crossings¹². Finally, bands of sufficient width along the edges were cut out to avoid edge effects induced by the displacement field.

The skewness with this approximate dynamics

The skewness of the projected density is given by the skewness of the 2D dynamics (Munshi et al. 1997), that is,

$$s_3^{\text{density}} = \frac{36}{7} + \frac{3}{2} \frac{d \log \sigma^2(\theta)}{d \log \theta}. \quad (37)$$

The skewness for the convergence would then simply be,

$$s_3^{\text{convergence}} = \frac{1}{\bar{\omega}} \left(\frac{36}{7} + \frac{3}{2} \frac{d \log \sigma^2(\theta)}{d \log \theta} \right). \quad (38)$$

This result is to be compared with the results obtained in BvWM. Their general formula (67) contains some extra geometrical factors of order unity (coming from the fact that averages along the line of sights are made in slightly different manners in the two cases). The Eq. (38) actually corresponds to the approximate form of Eq. (75) of BvWM.

Shapes and normalizations of the power spectra

The 3D power spectrum given by Baugh & Gaztañaga (1996) (BG spectrum) is used in most of our simulations,

$$P(k) \propto \frac{k}{[1 + (k/k_c)^2]^{3/2}}, \quad (39)$$

where $k_c = 0.05 h_{100} \text{Mpc}^{-1}$. In a series of simulation we used the standard CDM spectrum to compared with this model.

In most cases the fluctuations are normalized according to the convergence field $\langle \sigma_\kappa \rangle = C \sigma_e$. The value of σ_8 that has been chosen thus depends on Ω_0 in such a way that it is equal to 0.6 for a flat Universe (following the

¹² However, in the open cases it very rarely happened that κ reached unrealistic large values. The amplitude of κ has therefore been arbitrarily limited to 0.1. At most a handful of pixels have been affected by this cut-off.

normalization inferred from galaxy cluster counts, Eke et al. 1996, Oukbir & Blanchard 1997). As a result we take,

$$\sigma_8 = 0.6 \frac{\bar{\omega}(\Omega_0 = 1)}{\bar{\omega}(\Omega_0)} \quad (40)$$

It implies that the values of σ_8 grows for low values of Ω . Note that since $\bar{\omega} \approx \Omega^{-0.8}$, this growth is only slightly more important in our case than for the galaxy cluster counts (the exponent would be about 0.5 to 0.6).

Appendix B

This appendix gives the details of the reconstruction algorithm, how the g map is generated from an initial κ map, and the noise model.

Reconstruction algorithm

The lensing quantities of interest are defined in the Eqs.(6), and the observable is the reduced shear $g = \gamma/(1 - \kappa)$. The reconstruction problem is how to infer the κ map from an observed ellipticity field ϵ_{obs} , knowing that $\langle \epsilon_{obs} \rangle = -g$ is an unbiased estimate of the reduced shear? Note that this problem is under-constrained since a change in the potential ψ of the form,

$$\psi \rightarrow \lambda\psi + \frac{(1 - \lambda)}{2} |\theta|^2, \quad (41)$$

where λ is a constant, leaves unchanged the reduced shear g , but will transform the convergence as $\kappa \rightarrow \lambda\kappa + 1 - \lambda$ (see Seitz et al. 1998). This is the so called mass-sheet degeneracy. Thus in order to get a realistic convergence map, λ has to be determined by forcing $\bar{\kappa} = 0$ at the survey scale. The estimate of κ is obtain by a non-parametric least χ^2 method (Bartelmann et al. 1995). The image is sampled on a $N \times N$ grid, and the potential on a $(N + 1)^2$ grid. Starting from a guess on ψ , a guess on the reduced shear is derived and the following function is minimized with respect to ψ ,

$$\chi^2 = \sum_{ij} |g_{\text{guess}} - g|^2. \quad (42)$$

The finite difference schemes which are used in order to calculate the second derivatives of the potential at pixel (i, j) are,

$$\begin{aligned} \psi_{11}(i, j) &= [\psi(i + 2, j) + \psi(i - 2, j) - 2\psi(i, j)] / 4 \\ \psi_{22}(i, j) &= [\psi(i, j + 2) + \psi(i, j - 2) - 2\psi(i, j)] / 4 \\ \psi_{12}(i, j) &= [\psi(i + 1, j + 1) - \psi(i + 1, j - 1) \\ &\quad - \psi(i - 1, j + 1) + \psi(i - 1, j - 1)] / 4. \end{aligned} \quad (43)$$

We found that these schemes give the best regularization at small scales and avoid the usual high frequency oscillations in crude reconstruction schemes. At the edges of

the field the shift of 2 pixels in Eqs. (43) must be only one pixel in the direction perpendicular to the border since the potential is sampled on a $(N + 1)^2$ grid only. This has the consequence to slightly increase the noise at the boundaries but does not produce any bias. Once Eq. (42) is minimized, the κ map is found, and then the condition $\bar{\kappa} = 0$ is imposed on it.

Construction of the initial g map

A problem that we have to solve in this work is how to get the shear pattern of a projected mass distribution? Namely from the simulated κ we want to get the corresponding distortion map, put a noise on it, and reconstruct κ . The construction of a distortion map from a convergence map is unfortunately an under-constrained problem again. For example any transformation of the potential $\psi \rightarrow \psi + \bar{\psi}$ with $\Delta\bar{\psi} = 0$ leaves the convergence unchanged, but may change the shear (such a solution is for example $\theta_x^2 - \theta_y^2 + \theta_x\theta_y$). A peculiar solution for the potential ψ can be obtained by minimizing the χ^2 function:

$$\chi^2 = \sum_{ij} (\kappa - \kappa_{\text{guess}})^2. \quad (44)$$

The resulting reduced shear is then $g + \bar{g}$, where \bar{g} is the unphysical solution given by $\bar{\psi}$, but it is possible to reconstruct the convergence using Eq.(13), since κ is unchanged by the presence of the term \bar{g} . Unfortunately it is no longer the case when the noise is included via Eq.(10), because \bar{g} explicitly comes in the denominator. Fortunately, the role of the denominator in Eq.(10) is weak (this is a one percent effect on each galaxy if we take $g \simeq \bar{g} \simeq 0.01$ and $\epsilon^{(s)} \simeq 0.1$), this is in particular one of the reasons why the weak lensing approximation works so well. We thus did not try to correct for the presence of a spurious contribution \bar{g} in all the calculations, since it gives a negligible contribution to the signal (in terms of power spectrum and moments).

Noise generation

Once the true g maps are obtained the noise is introduced in a realistic way, using Eq.10: a sample of background galaxies with random intrinsic orientations is sheared, from which the κ map is reconstructed. The galaxies are observed in a grid of *superpixels* of 2.5 arcmin size (the minimum size of the κ map simulations), in which the number of galaxies N_i per superpixel i is known. In principle this number suffers of the amplification bias (depending on the line of sight matter quantity), but this effect is neglected here. N_i follows a Gaussian distribution of mean N_p and variance $\sqrt{N_p}$. Each pixel i of the image gives a local estimate of the reduced shear from the N_i galaxies, each of them having an intrinsic ellipticity $\epsilon_j^{(s)}$ which contributes as a source of noise for the shear signal.

The distribution of $\epsilon_j^{(s)}$ is a truncated normalized Gaussian defined over the range $[0, 1]$,

$$p(\epsilon_j^{(s)}) \propto \exp \left(- \left(\frac{\epsilon_j^{(s)}}{\sigma_\epsilon} \right)^2 \right), \quad (45)$$

where we choose $\sigma_\epsilon = 0.12$. (which corresponds to a typical axis ratio of 0.8).

From Eq. (10), the observed mean ellipticity $\bar{\epsilon}_i$ of a number N_i of galaxies in the image plane is given by,

$$\bar{\epsilon}_i = \frac{1}{N_i} \sum_{j=1}^{N_i} \frac{\epsilon_j^{(s)} - g}{1 - g^* \epsilon_j^{(s)}}. \quad (46)$$

Where $\bar{\epsilon}_i$ is an unbiased estimate of the reduced shear g in the superpixel i (Schramm & Kayser 1995, Schneider & Seitz 1995). A realistic estimate of N_p depends on the observational context, the telescope used, the optical filter, the atmospheric conditions,... By choosing $N_p = 30$ gal/arcmin² or 50 gal/arcmin² we adopted a conservative and reasonable assumption about the telescope time: the former is accessible in the I-band with 1.5 hour integration at CFHT, while the later is accessible for 4 hours in the same conditions.